ADM-AEOLUS LEVEL-2B ALGORITHM THEORETICAL BASELINE DOCUMENT

(MATHEMATICAL DESCRIPTION OF THE AEOLUS LEVEL-2B PROCESSOR)

Authors

David TAN, Erik ANDERSSON
ECMWF

Paul POLI, Alain DABAS
MÉTÉO-FRANCE

Jos De KLOE, Gert-Jan MARSEILLE, Ad STOFFELEN
KNMI

CHANGE LOG

Issue.	Date	New pages	Modified pages (after introducing new pages)	Observations	Name
0.1	25.11.2005	--	--	First draft	Poli, Tan
0.2	22.12.2005	29-31,32-33	16,21-22,23	Further details: centre-of-gravity height referenced to geoid, tripod obscuration correction in Mie processing, error quantifiers.	Tan
0.3	06.07.2006			Revisions to Mie Hlos error (Section 17).	Dabas
0.4	25.07.2006			L1B Screening, Retrieval of optical properties	Marseille
1.0	13.09.2006			Editorials	Tan
2.0	05.12.2006			Main title “Algorithm Theoretical Baseline Document”. Details of Sections 7-10.	Tan de Kloe Stoffelen
2.1	23.12.2007			Description of Matchup. Comments from ESA. Change bars with respect to Issue 2.0.	de Kloe Tan

Table of Contents

1. Introduction

The present document is the Algorithm Theoretical Baseline Document for the ADM-Aeolus Level-2B Processor. It is evolved from Technical Note 2.3 (issue 1.0) of the contract study "Development and Production of Aeolus Wind Data Products" which content is fully described in [AD2]. It provides a mathematical description of the baseline algorithm for Aeolus Level-2B (L2B) processing. Future versions of this ATBD shall

- provide justification for algorithm and parameter choices,
- identify open problems, and
- specify future developments.

The nature of the parameters of L2B products is described in [RD6]. File formats for L2B product and associated auxiliary data are described in [RD10]. The high-level architecture of L2B processing is described in [RD8].

2. Documents

2.1. Applicable documents

Ref	Document title	Document ref	Ver	Date
[AD1]	Statement of Work of the Development and Production of L2B/C Aeolus data.	AE-SW-ESA-GS-0117	1B	Sep 2004
[AD2]	Answer to RFQ/3-11094/04/NL/MM.			Jul 2004
[AD3]	PDS to ECMWF: Interface Control Document.	XADM-GSEG-EOPG-ID-04-0002	1.5	Oct 2006
[AD4]	Implementation of Level 2B/2C Processing Facility. Technical Requirements	XADM-GSEG-EOPG-RD-04-0003	1.1	Jun 2004
[AD5]	Earth Explorer Ground Segment File Format Standard	PE-TN-ESA-GS-001	1.4	Jun 2003

2.2. Reference documents

Ref	Document title	Document ref	Ver	Date
[RD1]	Aladin Instrument Operation Definition	AE-TN-ASF-AL-00044	3.0	Oct 2004
[RD2]	REMOVED			
[RD3]	Level1B Master Algorithm Document	AE-SW-ASU-GS-023	4.0	Jun 2006
[RD4]	Impact of line shape on wind measurements and correction methods	AE-SW-ESA-GS-016	1.0	Feb 2004
[RD5]	L1B & E2S Input/Output Data Definitions Interface Control Document	ADM-IC-52-1666	3.2	Jan 2007
[RD6]	Selection of L2B Parameters (Study TN2.1)	AE-TN-MFG-L2P-0021	1.2	Sep 2005
[RD7]	Aeolus Data Products Contents Guidelines	AE-TN-ESA-SY-007	1B	May 2004
[RD8]	Definition of Baseline Aeolus Level-2B Processing (Study TN2.2)	AE-TN-ECMWF-L2P-0022	1.2	Sep 2005
[RD9]	Level 1b Processor Detailed Processing Model	ADM-MA-52-1800	1/2	Sep 2005
[RD10]	ADM-Aeolus Level-2B Processor Input/Output Data Definitions Interface Control Document	AE_IF_ECMWF-L2BP-001	1.3	Feb 2007
[RD11]	Aeolus Product Modification for Implementation in L1bP CodeV2	AE.TN.DLR.APM-L1B.150206	1.3	Feb 2006

2.3. Acronyms

ACCD Accumulation Charge Coupled Device
AMD Auxiliary Meteorological Data

AOCS	Attitude and Orbit Control System
BRC	Basic Repeat Cycle
DEM	Digital Elevation Map
E2S	End-to-End Simulator
ECMWF	European Center for Medium-Range Weather Forecast
EE	Earth Explorer
(H)LOS	(Horizontal) Line Of Sight
L1B	Level-1B
L2B	Level-2B
L2C	Level-2C
MPH	Main Product Header
NRT	Near Real Time
NWP	Numerical Weather Prediction
ODB	Observation DataBase
PDS	Payload Data Segment
PRF	Pulse Repetition Frequency
QRT	Quasi Real Time
SNR	Signal to Noise Ratio
SPH	Specific Product Header
WGS84	World Global System 84: Reference Ellipsoid for GPS data.
WMO	World Meteorological Organization

3. Overview of Level-2B processing modes

3.1. Purpose of Level-2B processing

Level-2B processing is required to facilitate the production of L2B data products. As explained in TN2.1, i.e. [RD6], L2B products are intermediate between L1B and L2C products. Level-2B processing comprises primary Level-2B processing ("HLOS retrieval") and auxiliary Level-2B processing:

- Primary Level-2B processing ("HLOS retrieval"): involves taking L1B products, auxiliary input parameters and auxiliary meteorological data, and applying essential modifications, corrections and additions as a prelude to the assimilation of ADM-Aeolus observations by the NWP systems of ECMWF and other meteorological centres.
- Auxiliary Level-2B processing: involves the generation/acquisition of auxiliary meteorological data as required for HLOS retrieval. The auxiliary meteorological data take the form of *a priori* information on the state of the atmosphere at the time and place of L1B observations (with provision for late-arriving L1B observations where necessary).

Three principal modes of Level-2B processing are envisaged [e.g. RD6]. These are:

- the operational mode (at ECMWF);
- the met-centre mode; and
- the re-processing mode.

The met-centre mode is envisaged primarily for meteorological centres that i) have timeliness constraints that differ substantially from the ECMWF operational schedule, and ii) are able to undertake their own auxiliary L2B processing.

At the time of writing, all Chapters of this document are applicable to all modes of the L2BP. However, Appendix A describes auxiliary processing as defined for the operational mode only.

All three Level-2B processing modes are intended to support L1B input comprising parts of an orbit, a full orbit, or more than one orbit.

4. High-level architecture of Level-2B processing

The high-level architecture of Level-2B processing is described in [RD8], from which Figures 1 and 2 have been repeated to show data flow between the main processing tasks. A common design has been adopted for the three principal processing modes. Figure 1 shows the data flow and main processing tasks of auxiliary L2B processing and the link to primary L2B processing, i.e. HLOS retrieval, which is shown in Figure 2.

The breakdown of tasks has been designed so that the need for different software in operational, met-centre and pre-processing modes is largely confined to the auxiliary processing steps (Figure 1). This maximizes the portability of the code for primary L2B processing (Figure 2), which will permit different processing modes to exercise different options through appropriate settings in auxiliary parameter input files.

[RD8] explains that the aspects of Figure 1 that are not expected to apply in met-centre mode are a) the sending of data to the Core PDS, and b) the use of predicted flight tracks. Met centres are free to modify the other aspects of auxiliary processing to suit their own requirements (see [RD8] for further guidance).

[RD8] also explains that the dashed box in Figure 1 is not applicable to re-processing mode. Instead, auxiliary meteorological data at reference locations (before interpolation to locations requested by the HLOS retrieval algorithm) are to be obtained from the archive within the Core PDS. The re-processing mode will apply auxiliary preprocessing as described in Appendix A.3, consistent with the operational mode.

A high-level description of the main processing tasks is given in Section 5.

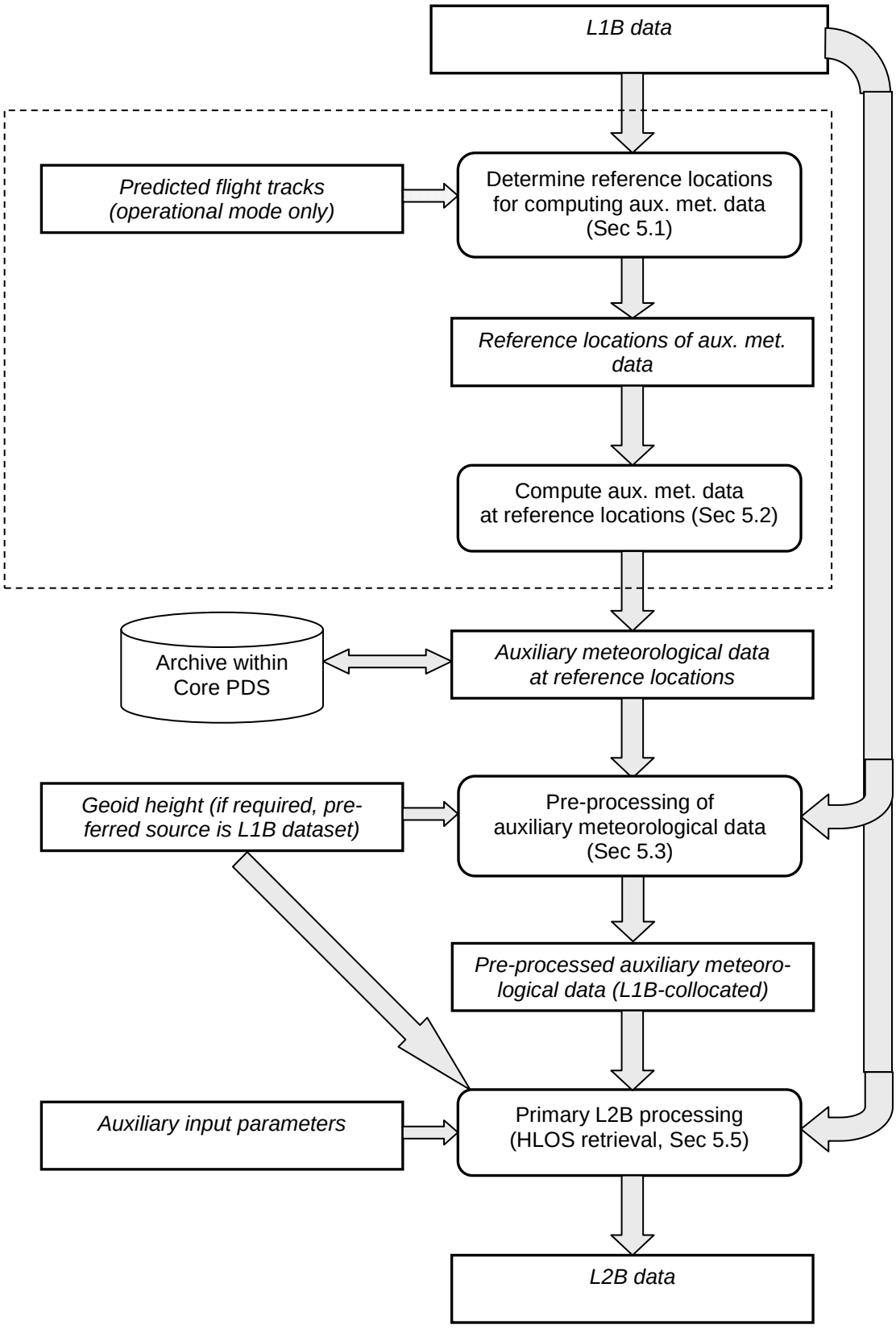

Figure 1: Data flow for ADM-Aeolus Level-2B processing. All the steps before HLOS retrieval comprise Auxiliary L2B processing in operational mode. Reprocessing mode does not involve the dashed box. Met-centre mode may involve variations to auxiliary L2B processing. Data flow for primary Level-2B processing (i.e. HLOS retrieval) is given in Figure 2.

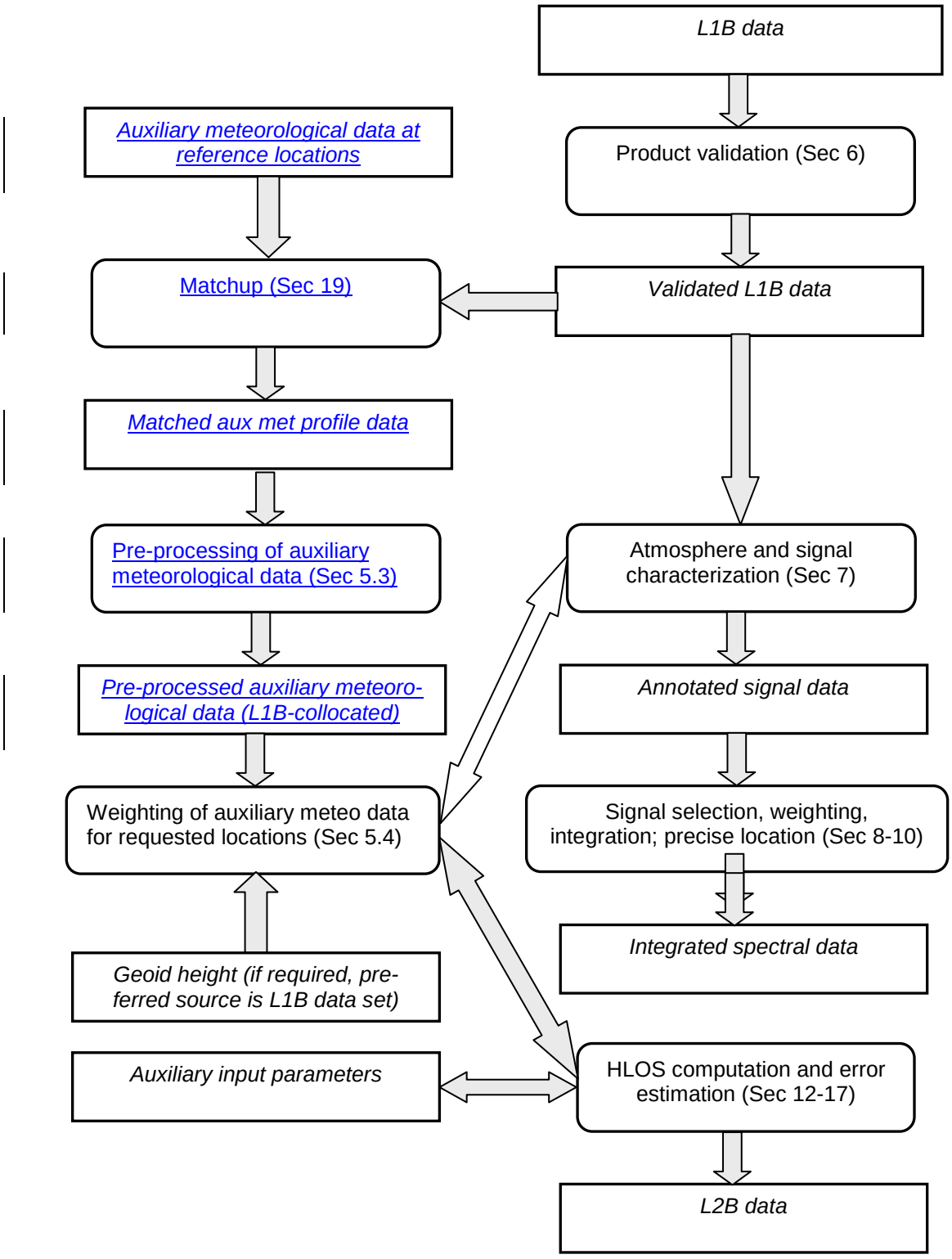

Figure 2: Data flow for ADM-Aeolus Primary Level-2B processing (HLOS retrieval)

5. Main processing tasks

The main mathematical description of the processing tasks is given in Chapters 6 to 17. To show the correspondence with the high-level architecture given in [RD8], we repeat in subsections 5.1 to 5.5 below the task headings from [RD8] and indicate the corresponding sections where the mathematical description is presented. A simpler correspondence between the high-level architecture and the mathematical description is expected before launch, taking into account results from pre-launch campaign and validation activities, and should be reflected in future updates of both this document and [RD8].

Notation: N = number of measurements in one BRC.

5.1. Determine reference locations for computing auxiliary meteorological data

This is part of auxiliary processing and is described in the Appendix A.1.

Note: determining reference locations is a preprocessing step performed outside the primary L2BP processing code. The L2BP main program has a preprocess option at the moment which can be used for this step. It reads the L1B file and provides an ASCII file describing the lat,lon,date,time values for which auxiliary meteorological data is needed. This is intended as an example. Met centers that wish to run the L2BP as a separate executable may adapt this code to their needs (and produce their own ASCII or otherwise formatted file to do this).

Also note that this preprocessing may be moved in a future update to its own dedicated executable program.

5.2. Generate auxiliary meteorological data at reference locations

This is part of auxiliary processing and is described in the Appendix A.2.

5.3. Pre-process auxiliary meteorological data

This is part of auxiliary processing and is described in the Appendix A.3.

5.4. Weighting of auxiliary meteorological data for requested locations

This has been implemented for reference pressure and temperature as described in Section 11.3.

5.5. Primary L2B processing (HLOS retrieval)

The steps of primary L2B processing are described in separate chapters:

- Product validation, Chapter 6
- Atmosphere and signal characterization, Chapter 7
- Measurement selection, Chapter 8
- Weighting, Chapter 9
- Integration, Chapter 10
- Computations of L2B parameters (part 1), Chapter 11
  - centre-of-gravity
  - representative integration length
  - reference pressure and temperature
- Computations of L2B parameters (part 2: HLOS computation and error estimation), comprising
  - Rayleigh channel HLOS processing, Chapter 12 and 14
  - Mie channel HLOS processing, Chapter 13 and 15
  - Rayleigh channel error processing, Chapter 16
  - Mie channel error processing, Chapter 17.

6. Product Validation

Product validation comprises
- Screening of Level-1B Data Input Product
- Screening of Auxiliary Meteorological Data Input Product
- Screening of Rayleigh-Brillouin Calibration Data Input Product
- Screening of Climatological Data Input Product
- Screening of Calibration Coefficient Data Input Product

6.1. Screening of Level-1B Data Input Product

In the L1B-screening procedure, L1B input parameter values are checked on their validity, i.e. whether they fit in a pre-defined range of valid values. The output is a set of L2B screening parameters indicating the result (fail or pass) of the screening procedure.

The L2B screening output parameters include
- L1B_Screening_Obs_Screening for screening of L1B PCD data on observation scale
- L1B_Screening_Mie_Meas_Meas_QC for screening of L1B PCD Mie data on measurement profile scale
- L1B_Screening_Mie_Meas_Bin_Screening_Bin_QC for screening of L1B PCD Mie data on measurement range bin scale
- L1B_Screening_Rayl_Meas_Meas_QC for screening of L1B PCD Rayleigh data on measurement profile scale
- L1B_Screening_Rayl_Meas_Bin_Screening_Bin_QC for screening of L1B PCD Rayleigh data on measurement range bin scale

The values of the L2B screening output parameters are determined by the values of L1B input and the corresponding lower and upper threshold values of these parameters. In case of a missing parameter or failure of the threshold test, the failure is reported and the L2B screening output parameter is flagged. A threshold failure is reported when the parameter value is *larger than* a pre-defined upper threshold value or *smaller than* a pre-defined lower threshold value. The L1B input parameters and corresponding threshold values are described in Tables 1-5.

Table 1: L1B screening on observation scale. The L1B parameters correspond to the parameters in Table 2-20 of the L1B-IODD [RD11]. Thresholds given by a symbolic name refer to parameters in the AUX_PAR_2B processing parameters file. In case of a screening failure the numerical value of the L2B parameter L1B_Obs_Screening (See table 17 of [RD10]) is set to the corresponding value in the first column of Table 18 of [RD10].

L1B parameter	Lower threshold	Upper threshold
Laser related:		
L1B_Laser_Freq_Unlocked	0	L1B_Laser_Freq_Unlocked_Thresh
L1B_Ref_Pulses_Unlocked	0	L1B_Ref_Pulses_Unlocked_Thresh
L1B_Laser_Freq_Offset	0	L1B_Laser_Freq_Offset_Thresh
L1B_Laser_UV_Energy	0	L1B_Laser_UV_Energy_Thresh
L1B_ Laser_Freq_Offs_Stdev	0	L1B_Laser_Freq_Offs_StdevThresh
L1B_ Laser_UV_Energy_Stdev	0	L1B_Laser_UV_Energy_StdevThresh
L1B_Mie_Mean_Emit_Freq	L1B_Mie_Mean_Emit_Freq_Min	L1B_Mie_Mean_Emit_Freq_Max
L1B_ Mie _Emit_Freq_Stdev	0	L1B_Mie_Emit_Freq_Stdev_Thresh
L1B_Rayl_Mean_Emit_Freq	L1B_Rayleigh_Mean_Emit_Freq_Min	L1B_Rayleigh_Mean_Emit_Freq_Max
L1B_ Rayl _Emit_Freq_Stdev	0	L1B_RayleighEmitFreqStdevThresh
Satellite related		
L1B_Sat_Not_on_Target	0	L1B_Sat_Not_on_Target_Thresh

Measurement related		
L1B_Mie_Invalid_Meas	0	L1B_Mie_Corrupt_Thresh
L1B_Mie_Invalid_Ref_Pulses	0	L1B_Mie_Ref_PulsesCorruptThresh
L1B_Rayl_Invalid_Meas	0	L1B_Rayleigh_Corrupt
L1B_Rayl_Invalid_Ref_Pulses	0	L1B_Rayl_RefPulsesCorruptThresh
Combinations		
L1B_Mie_Invalid_Meas	0	L1B_Mie_Invalid_Meas_Thresh
L1B_Mie_ Invalid_Ref_Pulses	0	L1B_Mie_Invalid_RefPulsesThresh
L1B_Rayl_Invalid_Meas	0	L1B_Rayl_Invalid_Meas_Thresh
L1B_Rayl_ Invalid_Ref_Pulses	0	L1B_Rayl_InvalidRefPulsesThresh

Table 2: L1B screening of Mie data on measurement scale. The L1B parameters correspond to the parameters in Table 2-25 of the L1B-IODD [RD11]. Thresholds given by a symbolic name refer to parameters in the AUX_PAR_2B processing parameters file. In case of a screening failure the numerical value of the L2B parameter L1B_Mie_Meas_QC (See table 19 of [RD10]) is set to the corresponding value in the first column of Table 20.

L1B parameter	Lower threshold	Upper threshold
L1B_Mie_Meas_Invalid_Ref_Pulses	0	L1B_MieMeasInvalidRefPlssThresh
L1B_Avg_Laser_Freq_Offset	L1B_Avg_Laser_Freq_Offset_Min	L1B_Avg_Laser_Freq_Offset_Max
L1B_Avg_UV_Energy	L1B_Avg_UV_Energy_Min	L1B_Avg_UV_Energy_Max
L1B_Laser_Freq_Offset_Stdev	0	L1B_Laser_FreqOffsetStdevThresh
L1B_UV_Energy_Std_Dev	0	L1B_UV_Energy_Stdev_Thresh
L1B_Vel_of_Att_Uncertainty_Error	L1B_VelofAttUncertaintyErrorMin	L1B_VelofAttUncertaintyErrorMax
L1B_Mie_Mean_Emitted_Freq	L1B_Mie_Mean_Emitted_Freq_Min	L1B_Mie_Mean_Emitted_Freq_Max
L1B_Mie_Emitted_Freq_Stdev	This parameter is no longer screened (removed in L1B v1.3)	
L1B_Reference_Pulse_FWHM	New parameter added in L1B v1.3; no thresholds defined yet in the code.	

Table 3: L1B screening of Mie data on range bin scale scale. The L1B parameters correspond to the parameters in Table 2-27 of the L1B-IODD [RD11]. Thresholds given by a symbolic name refer to parameters in the AUX_PAR_2B processing parameters file. In case of a screening failure the numerical value of the L2B parameter L1B_Mie_Meas_QC (See table 21 of [RD10]) is set to the corresponding value in the first column of Table 22. The logical parameter has been set by L1BP and is either true (T) or false (F).

L1B parameter	Lower threshold	Upper threshold	logical
L1B_Mie_Bin_Invalid	-	-	T/F
L1B_Scattering_Ratio	L1B_ScatteringRatio_Min	L1B_ScatteringRatio_Max	-
L1B_Mie_SNR	L1B_Mie_SNR_Thresh	No upper threshold	-

Table 4: L1B screening of Rayleigh data on measurement scale. The L1B parameters correspond to the parameters in Table 2-25 of the L1B-IODD [RD11]. Thresholds given by a symbolic name refer to parameters in the AUX_PAR_2B processing parameters file. In case of a screening failure the numerical value of the L2B parameter L1B_Rayleigh_Meas_QC (See table 23 of [RD10]) is set to the corresponding value in the first column of Table 24.

L1B parameter	Lower threshold	Upper threshold
L1B_Rayl_Meas_Invalid_Ref_Pulses	0	L1B_RayMeasInvalidRefPlssThresh
L1B_Avg_Laser_Freq_Offset	L1B_Avg_Laser_Freq_Offset_Min	L1B_Avg_Laser_Freq_Offset_Max
L1B_Avg_UV_Energy	L1B_Avg_UV_Energy_Min	L1B_Avg_UV_Energy_Max
L1B_Laser_Freq_Offset_Stdev	0	L1B_Laser_FreqOffsetStdevThresh
L1B_UV_Energy_Std_Dev	0	L1B_UV_Energy_Stdev_Thresh
L1B_Vel_of_Att_Uncertainty_Error	L1B_VelofAttUncertaintyErrorMin	L1B_VelofAttUncertaintyErrorMax
L1B_Rayleigh_Mean_Emitted_Freq	L1B_Rayl_Mean_Emitted_Freq_Min	L1B_Rayl_Mean_Emitted_Freq_Max
L1B_Rayleigh_Emitted_Freq_Stdev	0	L1B_Rayl_EmittedFreqStdevThresh

Table 5: L1B screening of Rayleigh data on range bin scale scale. The L1B parameters correspond to the parameters in Table 2-27 of the L1B-IODD [RD11]. Thresholds given by a symbolic name refer to parameters in the AUX_PAR_2B processing parameters file. In case of a screening failure the numerical value of the L2B parameter L1B_Rayleigh_Bin_QC (See table 25 of [RD10]) is set to the corresponding value in the first column of Table 26. The logical parameter has been set by L1BP and is either true (T) or false (F).

L1B parameter	Lower threshold	Upper threshold	logical

L1B_Rayleigh_Meas_Bin_Invalid	-	-	T/F
L1B_Rayleigh_SNR_A	L1B_Rayleigh_SNR_Min	L1B_Rayleigh_SNR_Max	-
L1B_Rayleigh_SNR_B	L1B_Rayleigh_SNR_Min	L1B_Rayleigh_SNR_Max	-

6.2. Screening of Auxiliary Meteorological Data Input Product

TBD.

6.3. Screening of Rayleigh-Brillouin Calibration Data Input Product

TBD.

6.4. Screening of Climatological Data Input Product

TBD.

6.5. Screening of Calibration Coefficient Data Input Product

TBD.

7. Atmosphere and Signal Characterization

The principal task of atmospheric characterization is to establish a set of atmospheric classes representative of the measurements within the BRC. This is referred to below as “scene classification”, and details are given in Section 7.2.

It is envisaged that atmosphere and signal characterization will support the following three modes of operation, each with mode-specific algorithms:

1) Fabry-Perot only
2) Fizeau only
3) Combined Fabry-Perot and Fizeau atmospheric characterization

Some of these algorithms require, as a preliminary step, the retrieval of atmospheric optical properties to be undertaken during Level-2B processing.

7.1. Retrieval of atmospheric optical properties

Inputs:

Algorithm selection parameters - from AUX_PAR_2B processing parameters file

Additional parameters depending on the methods applied - see sub-sections of Section 18

Outputs:

Particle optical thickness for every Mie measurement bin

Particle optical thickness for every Rayleigh measurement bin

Scattering ratio for every Mie measurement bin

Scattering ratio for every Rayleigh measurement bin

Additional parameters depending on the methods applied - see sub-sections of Section 18

Algorithm:

The algorithms for atmosphere and signal characterization are underpinned by a geophysical model of the atmospheric return signal, as given in Appendix C.

Atmosphere characterization is based on the retrieval of atmospheric optical properties. A number of alternative algorithms are given in Section 18.

Some of these algorithms depend on the provision of signal calibration constants. It is currently assumed that these will be available in the input data (files) to the L2B processor. Some algorithms for checking the supplied values during L2B processing are given in Appendix D.

The retrieval of atmospheric optical properties provides input to the scene classification (feature-finding) algorithm.

7.2. Scene classification

7.2.1. Atmospheric Characterization Algorithm-1 (Fabry-Perot only):

No atmospheric characterization implemented yet.

7.2.2. Atmospheric Characterization Algorithm-2 (Fizeau only):

No atmospheric characterization implemented yet.

7.2.3. Atmospheric Characterization Algorithm-3 (Combined Fabry-Perot and Fizeau):

In the combined Fabry-Perot and Fizeau atmospheric characterization option, the L1B backscatter ratio estimate is used to classify the atmospheric scene at the measurement scale. An atmospheric class is assigned to each measurement bin. In the current implementation, valid atmospheric classes are:

- Cloud (encompassing both cloud and aerosol)
- No-cloud

Inputs:

- L1B backscatter ratio
- L1B range gate altitude (top and bottom)
- Threshold profile as a function of altitude (from AUX_PAR_2B input file)

Outputs:

- Atmospheric class of each measurement bin

Algorithm:

The middle of the range gate, z_i, is determined from the average of the range gate top and bottom. Subsequently, a threshold value is determined from the threshold profile by linearly interpolating to the altitude z_i. If the L1B backscatter ratio exceeds the interpolated threshold, then the measurement bin's atmospheric class is set to Cloud, else it is set to No-cloud.

8. Measurement Selection

Measurement bins are attributed to observation sub-profiles distinguished by atmospheric class.
There is one observation sub-profile for each atmospheric class present in the BRC measurements.

Inputs:

- Atmospheric class of each measurement bin (from Section 7.2.3)

Outputs:

- Number of observation sub-profiles used in BRC
- Mapping of the measurements onto the observation sub-profiles

Algorithm:
Measurement bins are scanned for attributed atmospheric class and the number of classes found is stored. For each atmospheric class present in the BRC it is determined which measurements contribute. This is stored in a map structure.

9. Weighting

For each measurement bin a weight is determined for its contribution to the observation profile for the corresponding atmospheric class. Each measurement bin contributes to only one observation profile.

Inputs:

- Mapping of the measurements onto the observation profiles (Section 8)

Outputs:

- Map of measurement weights for each measurement range bin, i.e.
  Weights W(i,k) for every Mie measurement k, range bin i.

  Weights W(i,k) for every Rayleigh measurement k, range bin i.
- Count of measurements within each range gate of each observation profile

Baseline Weighting Algorithm:
At every range gate, each measurement bin is assigned a baseline weight within its corresponding observation profile as follows:

$$W_i = 1.$$

(As mentioned above, a measurement bin contributes only to a single observation profile. Equivalently, outside its observation class, the weight is zero and hence is not stored.)

Further refinements to the baseline weights are anticipated (Section 9.1). The details are likely to depend on SNR parameters reported in L1B products.

Moreover, the number of measurements contributing to an atmospheric class on a specific range gate level is counted.

NOTE: for more efficient storage, the weights written to the L2B output file are:

$$W^*_i = \mathrm{Int}[\, 1000 * W_i].$$

9.1. Refinement of the Baseline Weighting Algorithm

This section is reserved for further refinements to the baseline weighting algorithm above. The details are likely to depend on SNR parameters reported in L1B products.

10. Integration

Inputs:

- Map of measurement weights for each measurement range bin (Section 9)

Outputs:

- Multiple profiles of integrated spectral L1B data for each channel - Section 13.1
- Annotated L1B data (updated with, e.g., weight information)
- Precise location (L2B centre -of-gravity) - Section 11.1
- Representative horizontal integration length of L2B wind estimate - Section 11.2

11. Computation of L2B parameters (part 1)

11.1. Computation of centre-of-gravity

Inputs:

$\lambda_m(i,k)$ - measurement-bin latitude, reported in L1B products

$\phi_m(i,k)$ - measurement-bin longitude, reported in L1B products

$z^u{}_m(i,k)$ - measurement-bin upper altitude, reported in L1B products

$z^l{}_m(i,k)$ - measurement-bin lower altitude, reported in L1B products

z_{geoid} - geoid offset relative to WGS84 for the BRC, reported in L1B products

W(i,k) - weights, output from Weighting (Section 9)

Outputs:

$\lambda_{cog}(i)$ - centre-of-gravity latitude, reported in L2B products

$\phi_{cog}(i)$ - centre-of-gravity longitude, reported in L2B products

$z^{u/l}{}_{cog}(i)$ - centre-of-gravity upper/lower altitude relative to the geoid, reported in L2B products

$z^c{}_{cog}(i)$ - centre-of-gravity centroid altitude relative to the geoid, reported in L2B products

z_{geoid} - geoid offset relative to WGS84 for the BRC, reported in L2B products (repeat of L1B input value)

11.1.1. Implemented option

Centre-of-gravity geolocation is defined by the L1B measurement geolocation parameters for a centre-of-gravity measurement index denoted by $\bar{k}$ and defined by

$$\bar{k} = \mathrm{int}[\sum_{k=1}^{N} W(i,k)k]$$

where int[] denotes the integer part of a real number.

Let $\lambda_m(i,k)$ denote the latitude at measurement k, range bin i. Then the centre-of-gravity latitude is given by

$$\lambda_{cog}(i) = \lambda_m(i,\bar{k})$$

Similarly, let $\phi_m(i,k)$ denote the longitude at measurement k, range bin i. Then the centre-of-gravity longitude is given by

$$\phi_{cog}(i) = \phi_m(i,\bar{k})$$

Similarly, let $z^{u/l}{}_m(i,k)$ denote the altitude at upper/lower edge of measurement k, range bin i. Then the upper/lower edge of the centre-of-gravity altitude is given by

$$z^{u/l}{}_{cog}(i) = z^{u/l}{}_m(i,\bar{k}) - z_{geoid}$$

and the centre-of-gravity centroid (or mid-level) altitude is given by

$$z^{c}{}_{cog}(i) = 0.5(z^{u}{}_{cog}(i) + z^{l}{}_{cog}(i))$$

Note that L2B centre-of-gravity altitudes are given relative to the geoid height of each BRC, as provided in L1B input.

11.1.2. Backup option

Let $\lambda_m(i,k)$ denote the latitude at measurement k, range bin i. Then the centre-of-gravity latitude is given by

$$\lambda_{cog}(i) = \sum_{k=1}^{N} W(i,k)\lambda_m(i,k)$$

Similarly, let $\phi_m(i,k)$ denote the longitude at measurement k, range bin i. Then the centre-of-gravity longitude is given by

$$\phi_{cog}(i) = \sum_{k=1}^{N} W(i,k)\phi_m(i,k)$$

Similarly, let $z_m(i,k)$ denote the mid-level altitude at measurement k, range bin i:

$$z_m(i,k) = 0.5(z^{u}{}_m(i,k) + z^{l}{}_m(i,k))$$

Then the centre-of-gravity altitude is given by

$$z_{cog}(i) = \sum_{k=1}^{N} W(i,k) z_m(i,k) - z_{geoid}$$

Note that L2B centre-of-gravity altitude is given relative to the geoid height of each BRC, as provided in L1B input.

11.2. Computation of representative L2B-observation integration length

Inputs:

L_M - horizontal integration length of a single measurement, source TBD

W(i,k) - weights, output from Weighting (Section 9)

Outputs:

$L_R(i)$ - representative L2B-observation integration length, reported in L2B products

Let the mean measurement index be denoted by

$$\bar{k}(i) = \sum_{k=1}^{N} W(i,k)k$$

Then the representative integration length is given by

$$L_R(i) = \left\{ \frac{12}{N} \sum_{k=1}^{N} W(i,k)\left[k - \bar{k}(i)\right]^2 \right\}^{1/2} L_M$$

Here N is the number of measreremements in the BRC and L_M is the length of one measurement. [Calculation of L_M is TBD: in particular, a method is needed to distinguish (50/N) km from (67/N) km]. Note that $L_R(i)$ is a multiple of the weighted standard deviation of the measurement positions. The factor 12/N arises because the weights are normalized to have a maximum of unity; in the case that all N measurements have unit weight, $L_R(i)$ is N times L_M, i.e. the length of the BRC.

Note: representative integration length is not yet implemented.

11.3. Computation of reference pressure and temperature

Inputs:

$p_{nwp}(i,k)$, $T_{nwp}(i,k)$ - preprocessed meteorological data (Section 5.3)

$z_m(i,k)$ - measurement-bin mid-level altitude (Section 11.1.2)

z_{geoid} - geoid offset relative to WGS84 for the BRC, reported in L1B products

W(i,k) - weights, output from Weighting (Section 9)

Outputs:

$p_0(i)$, $T_0(i)$ - reference temperature and pressure, reported in L2B products

Computation of reference pressure and temperature is done in two steps. The first is a vertical coordination translation between WGS84 and NWP coordinates (producing intermediate values pm and Tm). The second is a weighted average in the horizontal.

The intermediate pressures and temperatures are given by

$$p_m(i,k) = p_{nwp}(i'(k),k)$$

$$T_m(i,k) = T_{nwp}(i'(k),k)$$

where $i'(k)$ is such that $z_m(i,k) - z_{geoid}$ lies between $z_{nwp}(i'(k))$ and $z_{nwp}(i'(k)-1)$. Note that this is effectively a nearest neighbour interpolation. The intention is to replace this with a linear or higher order interpolation.

Following the previous weighting expressions, the reference pressure is given by

$$p_o(i) = \sum_{k=1}^{N} W(i,k)\, p_m(i,k)$$

Similarly, the reference temperature is given by

$$T_o(i) = \sum_{k=1}^{N} W(i,k) T_m(i,k)$$

12. Rayleigh channel HLOS processing

Inputs:

A_m(i,k), B_m(i,k) - Measurement Useful Signal in Channels A and B, reported in L1B products

C_m(k), D_m(k) - Measurement Internal Reference in Channels A and B, reported in L1B products

$\rho_m(i,k)$ - measurement-bin scattering ratio, reported in L1B products

ERRM, RRSM, β - L1B Rayleigh internal reference processing parameters (provisional, pending refined internal reference treatment)

λ_0 laser wavelength, reported in L1B products (provisional, pending refined internal reference treatment)

φ elevation angle, reported in L1B products

$V_{LOSm}(k)$ - spacecraft LOS velocity at measurement level, reported in L1B products

$C_R, W_{GR}, fit_{Ray}(lat), W_{HR}, C_M, W_{GMR}, fit_{Mie}(lat), W_{HMR}$ - ground correction parameters, reported in L1B products (TBC)

T_0(i), p_0(i) - reference temperature and pressure (output from Section 11.3)

W(i,k) - weights, output from Weighting (Section 9)

Rayleigh-Brillouin correction data, reported in AUX_RBC auxiliary input products

Outputs:

v(i) - L2B Rayleigh HLOS wind component

$\partial LOS^0 / \partial T$, $\partial LOS^0 / \partial p$, $\partial LOS^0 / \partial R$, $\partial LOS^0 / \partial \rho$ - local derivatives of LOS^0, auxiliary outputs from ILIAD (Section 12.2/14)

The Rayleigh channel HLOS retrieval involves computation of

- the weighted Rayleigh response (Section 12.1),
- the ILIAD HLOS velocity (Section 12.2),
- two post-ILIAD correction terms (Section 12.3)
    - the weighted internal reference LOS velocity (Section 12.3.1),
    - the weighted spacecraft LOS velocity (Section 12.3.2),
- the post-ILIAD HLOS velocity (Section 12.4).

These are described separately below.

12.1. Computation of a weighted Rayleigh response

The weighted Rayleigh response needed as input to ILIAD is computed as follows. The weighted summation useful signal in Channels A and B are given by analogues of the quantities A2, B2 from L1B DPM eqn (103):

$$A_o(i) = \sum_{k=1}^{N} W(i,k) A_m(i,k)$$

$$B_o(i) = \sum_{k=1}^{N} W(i,k) B_m(i,k)$$

The weighted Rayleigh response is given by the analogue of L1B DPM r1ro(i), eqn (105):

$$r1r_o(i) = \frac{Ao(i) - Bo(i)}{Ao(i) + Bo(i)}$$

This is used as input to ILIAD (Section 12.2).

12.2. Computation of the ILIAD HLOS velocity

Following the previous weighting expressions, the meteorologically-weighted scattering ratio is given by

$$\rho_o(i) = \sum_{k=1}^{N} W(i,k) \rho_m(i,k)$$

The ILIAD scheme is applied to give

$$V_{ILIAD}(i) = V_{ILIAD}\left[r1ro(i), \rho_o(i); T_o(i), p_o(i) \right]$$

Further details are given in Chapter 14. This is used as input to post-ILIAD corrections (Section 12.4).

Additional outputs are the LOS sensitivity with respect to temperature and pressure α_P(i) and α_T(i). These must be multiplied by $1/\sin(\varphi)$ to produce the L2B output parameters HLOS sensitivity with respect to temperature and pressure.

12.3. Computation of post-ILIAD correction terms

Two steps are described in this section, in preparation for use in the post-ILIAD HLOS velocity (Section 12.4).

12.3.1. Computation of a weighted internal reference LOS velocity

Computation of a meteorologically-weighted internal reference LOS velocity $V_{INT}(i)$ is performed as follows. The weighted summation internal reference for Channels A and B are given by analogues of the quantities C2, D2 from L1B DPM eqn (104):

$$C_o(i) = \sum_{k=1}^{N} W(i,k) C_m(k)$$

$$D_o(i) = \sum_{k=1}^{N} W(i,k) D_m(k)$$

The raw weighted Rayleigh internal reference response and its value after nonlinearity correction are given by analogues of L1B DPM eqns (105) and (64):

$$r1r_o(0,i) = \frac{Co(i) - Do(i)}{Co(i) + Do(i)}$$

$$RRM_o(0,i) = r1r_o(0,i) - ERRM[r1r_o(0,i)]$$

NOTE: Nonlinearity correction is not yet implemented. The current plan is to implement the nonlinearity correction when the relevant calibration data (ERRM) are present in the L1B TDS. It can be done sooner (reading from AUX_RRC files) if necessary.

Next, the internal reference LOS velocity is given by

$$V_{INT}(i) = \frac{\lambda_0}{2}\left(\frac{RRMo(0,i) - \beta}{RRSM}\right)$$

This is used as input to post-ILIAD corrections (Section 12.4)

NOTE: the terms in the above equation for internal reference LOS velocity are currently set to placeholders that give the result $V_{INT}(i) = 0$. The expression for $VINT(i)$ will be revised in favour of one that applies an analogue of the ILIAD scheme to $RRMo(0,i)$. This revision is contingent on updates to the AUX_RBC file that is an input to the L2B processor.

12.3.2. Computation of a weighted spacecraft LOS velocity

The weighted spacecraft LOS velocity is given by

$$V_{LOS}(i) = \sum_{k=1}^{N} W(i,k) V_{LOSm}(k)$$

This is used as input to post-ILIAD corrections (Section 12.4).

12.4. Computation of the post-ILIAD HLOS velocity

The post-ILIAD Rayleigh HLOS estimate is given by the analogue of L1B DPM eqn (69)

$$v(i) = V_{ILIAD}(i) - \frac{1}{\sin(\varphi)}\left[V_{INT}(i) + V_{LOS}(i) + C_R W_{GR}\right]$$

This quanitity is reported in L2B products. Here, φ is the elevation angle and C_R and W_{GR} are the ground correction terms taken directly from the L1B product file.

Note: an upgrade of the ground return term is expected around November 2006, in line with Eqn 69 of [RD3], e.g.

$$V_{GR} = C_R W_{GR} + fit_{Ray}(lat) W_{HR} + C_M W_{GMR} + fit_{Mie}(lat) W_{HMR}$$

13. Mie channel HLOS processing

Inputs:

LID_m(i,j,k), INT_m(j,k) - Measurement and Internal Reference spectrometer counts at measurement-bin level, reported in L1B products

EMR_A, EMR_I - spectral nonlinearity corrections, reported in L1B products

MRS_A, MRS_I, α, δ - L1B Mie channel processing parameters

λ_0 laser wavelength, reported in L1B products

φ elevation angle, reported in L1B products

$V_{LOSm}(k)$ - spacecraft LOS velocity at measurement level, reported in L1B products

$C_M, W_{GM}, fit_{Mie}(lat), W_{HM}$ - ground correction parameters, reported in L1B products (TBC)

Mie core algorithm processing parameters - set in AUX_PAR_2B processing parameter file

W(i,k) - weights, output from Weighting (Section 9)

Outputs:

v(i) - L2B Mie HLOS wind component

The Mie channel HLOS retrieval involves

- computation of weighted Mie spectrometer readouts (Section 13.1),
  - the computation is performed for both the atmospheric signal and the internal reference
- computation of the raw response via the Mie core algorithm (Section 13.2),
  - the computation is performed for both the atmospheric signal and the internal reference
- spectral nonlinearity correction (Section 13.3)
  - the computation is performed for both the atmospheric signal and the internal reference
- computation of the core LOS velocity (Section 13.4)
- computation of two post-core correction terms
  - the weighted internal reference LOS velocity (Section 13.5.1)
  - the weighted spacecraft LOS velocity (Section 13.5.2),
- computation of the post-core HLOS velocity (Section 13.6).

These are described separately below.

13.1. Computation of weighted Mie spectrometer readouts

The weighted Mie spectrometer readouts needed as input to the Mie core algorithm are computed as follows. The weighted summation spectrometer readouts (before tripod obscuration correction) for the atmospheric signal and for the internal reference are given by analogues of the quantities LID_O, INT_O from L1B DPM eqn (53) and (54):

$$LID'_o(i,j) = \sum_{k=1}^{N} W(i,k) LID_m(i,j,k)$$

$$INT'_o(i,j) = \sum_{k=1}^{N} W(i,k) INT_m(j,k)$$

Tripod obscuration correction is applied within the L2B Mie Core algorithm.

13.2. Computation of the raw response via the Mie core algorithm

The Mie core algorithm is applied to produce the following outputs:

$$r1mo(i) = Mie\_Core\left[LID_o(i,j)\right]$$

$$r1mo_{INT}(i) = Mie\_Core\left[INT_o(i,j)\right]$$

Further details are given in Chapter 15.

13.3. Spectral nonlinearity correction

Spectral nonlinearity correction takes the same form as L1B DPM eqn (57) and (58):

$$Rm(i) = r1mo(i) - EMR_A\left[r1mo(i)\right]$$

$$Rm_{INT}(i) = r1mo_{INT}(i) - EMR_I\left[r1mo_{INT}(i)\right]$$

Note: spectral nonlinearity correction is implemented in the L2BP but is currently switched off pending updated MRC data in L1B Test Data Sets.

13.4. Computation of the core LOS velocity

Computation of a meteorologically-weighted core LOS velocity $V_{CORE}(i)$ is performed as follows.

Next, the core LOS velocity is given by

$$V_{CORE}(i) = \frac{-\lambda_0}{2}\left(\frac{Rm(i)-\alpha}{MRS_A}\right)$$

This is used as input to post-core HLOS velocity computation (Section 13.6).

Note: the term alpha is not implemented in order to obtain results similar to the L1B processor.

13.5. Computation of two post-core correction term

Two steps are described in this section, in preparation for use in the post-core HLOS velocity (Section 13.6).

13.5.1. Computation of the weighted internal reference LOS velocity

Computation of a meteorologically-weighted internal reference LOS velocity $V_{INT}(i)$ is given by

$$V_{INT}(i) = \frac{-\lambda_0}{2}\left(\frac{Rm_{INT}(i) - \delta}{MRS_I}\right)$$

This is used as input to post-core HLOS velocity computation (Section 13.6).

Note: the term delta is not yet implemented in order to obtain results similar to the L1B processor.

13.5.2. Computation of a weighted spacecraft LOS velocity

The weighted spacecraft LOS velocity is given by

$$V_{LOS}(i) = \sum_{k=1}^{N} W(i,k) V_{LOSm}(i,k)$$

This is used as input to post-core HLOS velocity computation (Section 13.6).

13.6. Computation of the post-core HLOS velocity

The post-core Mie HLOS estimate is given by the analogue of L1B DPM eqn (62)

$$v(i) = V_{CORE}(i) - \frac{1}{\sin(\varphi)}\left[V_{INT}(i) + V_{LOS}(i) + C_M W_{GM}\right]$$

This quanitity is reported in L2B products. Here, φ is the elevation angle and C_R and W_{GR} are the ground correction terms taken directly from the L1B product file.

Note: the terms α / MRS_A and δ / MRS_I are not currently implemented; this is equivalent to assuming that they cancel identically.

Note: an upgrade of the ground return term is expected around November 2006, in line with Eqn 62 of [RD3], e.g.

$$V_{GM} = C_M W_{GM} + fit_{Mie}(lat) W_{HM}$$

14. The ILIAD retrieval

Input:

The temperature and pressure correction scheme requires as input the following arrays:

- T_A and T_B, response curves for channels A and B, defined for
  - frequencies *freq* (vector of size n_{freq}) between [-*FSR*,+*FSR*] =[-10.95 GHz, +10.95 GHz] with a step *df* = 25 MHz
- *S*, three-dimensional array of size n_P . n_T . n_{fr} defined for
  - pressures P_{grid} (vector of size n_P) between [P_{min} = 10 hPa, P_{max} = 1100 hPa] with a step *dP* = 50 hPa,
  - temperatures T_{grid} (vector of size n_T) between [T_{min} = 170 K, T_{max} = 330 K] with a step *dT* = 1 K,
  - and frequencies *fr* (vector of size n_{fr}) between [-*FSR*-*USR*/2, +*FSR*+*USR*/2] = [-11.70 GHz, +11.70 GHz] with a step *df*
- *F*, three-dimensional array of size n_P . n_T . n_{RR}, defined for
  - pressures P_{grid},
  - temperatures T_{grid},
  - and responses *RR0* (vector of size n_{RR}) between [-0.5, +0.5] with a step *dRR*=0.01
- *fd*, vector of size *nfd*, detector frequencies between [-*USR*/2, +*USR*/2] = [-0.75 GHz, +0.75 GHz], with a step *df*

The correction algorithm processes the following inputs (vectors of size *n*):

- *RRmes*, responses derived from measurements
- ρ, scattering ratios derived from measurements
- *Pmod*, pressures obtained from auxiliary meteorological information
- *Tmod*, temperatures obtained from auxiliary meteorological information

Algorithm:

In what follows below we define an index *i* and loop from 1 to *n*.

Correction of the Rayleigh:

The algorithm searches the arrays:

- P_{grid} for the closest point to $P_{mod}(i)$; *iP* is found ($nP \geq iP \geq 1$)
- P_{grid} for the closest point immediately above $P_{mod}(i)$; iP^+ is found ($nP \geq iP^+ \geq 1$)
- P_{grid} for the closest point immediately below $P_{mod}(i)$; iP^- is found ($nP \geq iP^- \geq 1$)

- T_{grid} for the closest point to $T_{mod}(i)$; *iT* is found ($nT \geq iT \geq 1$)
- T_{grid} for the closest point immediately above $T_{mod}(i)$; iT^+ is found ($nT \geq iT^+ \geq 1$)

- T_{grid} for the closest point immediately below $T_{mod}(i)$; iT^- is found ($nT \geq iT^- \geq 1$)

- *RR0* for the closest point to $RR_{mes}(i)$; iR is found ($nRR \geq iR \geq 1$)
- *RR0* for the closest point immediately above $RR_{mes}(i)$; iR^+ is found ($nRR \geq iR^+ \geq 1$)
- *RR0* for the closest point immediately below $RR_{mes}(i)$; iR^- is found ($nRR \geq iR^- \geq 1$)

The algorithm then calculates the following derivatives:

- $\alpha_P(i) = \frac{df}{dP} = \frac{F(iP^+, iT, iR) - F(iP^-, iT, iR)}{P_{grid}(iP^+) - P_{grid}(iP^-)}$
- $\alpha_T(i) = \frac{df}{dT} = \frac{F(iP, iT^+, iR) - F(iP, iT^-, iR)}{T_{grid}(iT^+) - T_{grid}(iT^-)}$
- $\alpha_{RR} = \frac{df}{dRR} = \frac{F(iP, iT, iR^+ - F(iP, iT, iR^-)}{RR0(iR^+) - RR0(iR^-)}$

The temperature- and pressure-corrected frequency for the response RR_{mes}(i) is then calculated as:

$$f_{\mathrm{mod}} = F(iP, iT, iR) + \alpha_T(i) \cdot \left(T_{\mathrm{mod}}(i) - T_{grid}(iT)\right) + \alpha_P(i) \cdot \left(P_{\mathrm{mod}}(i) - P_{grid}(iP)\right) + \alpha_R \cdot \left(RR_{mes}(i) - RR0(iR)\right)$$

Correction of the Mie:

We form the following matrix:

$$S1 = \begin{bmatrix} S(iP, iT, 1) & S(iP, iT, 2) & \cdots & S(iP, iT, n_{freq}) \\ S(iP, iT, 2) & S(iP, iT, 3) & \cdots & S(iP, iT, n_{freq} + 1) \\ \vdots & \vdots & \ddots & \vdots \\ S(iP, iT, n_{fd} + 1) & S(iP, iT, n_{fd} + 2) & \cdots & S(iP, iT, n_{freq} + n_{fd} - 1) \end{bmatrix}$$

where the three-dimensional matrix *S* was calculated beforehand using the Tenti S6 model. We then multiply the matrix *S1* by the calibration response curves

$$N_A^{(1)} = df \cdot \left(S1 \cdot T_A\right)$$
$$N_B^{(1)} = df \cdot \left(S1 \cdot T_B\right)$$

and evaluate the response without the Mie effect on the detectors as

$$R^{(1)} = \frac{N_A^{(1)} - N_B^{(1)}}{N_A^{(1)} + N_B^{(1)}}$$ (vector of size n_{fd})

We then interpolate the range of frequencies *–fd* from the calculated responses $R^{(1)}$ to the measured response *RRmes*(i) using spline interpolation and obtain a frequency response *R1*. Finally, we calculate the expected counts without Mie contribution $T1_A$ and $T2_B$ given the response *R1* by interpolating the arrays T_A and T_B (respectively*)* from the frequency responses *freq* to *R1*.

In order to calculate the frequency responses with a Mie contribution, we first form the following matrix:

$$S2 = S1 + (\rho - 1) \cdot \begin{bmatrix} g_{Mie}(1) & g_{Mie}(2) & \cdots & g_{Mie}(n_{freq}) \\ g_{Mie}(2) & g_{Mie}(3) & \cdots & g_{Mie}(n_{freq}+1) \\ \vdots & \vdots & \ddots & \vdots \\ g_{Mie}(n_{fd}+1) & g_{Mie}(n_{fd}+2) & \cdots & g_{Mie}(n_{freq}+n_{fd}-1) \end{bmatrix}$$

where we have calculated beforehand the following parameters from the laser wavelength λ_0:

$FWHM = \frac{c \cdot 0.02 \cdot 10^{-12}}{\lambda_0^2}$ (*c* is the speed of light), $\sigma_{Mie} = \frac{FWHM}{2 \cdot \sqrt{\log(2)}}$ and

$g_{Mie} = \frac{1}{\sigma_{Mie} \cdot \sqrt{\pi}} \cdot \exp\left(-\frac{fr^2}{\sigma_{Mie}^2}\right)$ is a vector of size *nfr* defined for frequencies *fr*.

We apply the same steps as previously, namely:

$$N_A^{(2)} = df \cdot (S2 \cdot T_A)$$
$$N_B^{(2)} = df \cdot (S2 \cdot T_B)$$

$R^{(2)} = \frac{N_A^{(2)} - N_B^{(2)}}{N_A^{(2)} + N_B^{(2)}}$ (vector of size n_{fd})

We then interpolate the range of frequencies *–fd* from the calculated responses $R^{(2)}$ to the measured response *RRmes*(i) using spline interpolation and obtain a frequency response *R2*. Finally, we calculate the expected counts with Mie contribution $N2_A$ and $N2_B$ given the response *R2* by interpolating the arrays $N_A^{(2)}$ and $N_B^{(2)}$ (respectively*)* from the detector frequencies *fd* to *R2*.

We then evaluate the derivative of the frequency response with respect to the scattering ratio using:

$$\frac{df}{d\rho} = \frac{\frac{dR}{d\rho}}{\frac{dR}{df}}$$

where $\frac{dR}{d\rho} = \frac{T1_A - T1_B - RR_{mes}(i) \cdot (T1_A + T1_B)}{N2_A + N2_B}$

and $\frac{dR}{df} = f2^+ - f2^-$ where $f2^+$ ($f2^-$) is obtained by interpolating *R2*+1 (*R2*, respectively) from *–fd* to $R^{(2)}$.

After correction for the pressure and the temperature of the Rayleigh and Mie contributions, the Doppler frequency shift is then:

$$f_{cor} = f_{\mathrm{mod}} + (1 - \rho) \cdot \frac{df}{d\rho}$$

The wind velocity is computed from the Doppler frequency shift as:

$$u(i) = -f_{cor} \cdot \frac{\lambda_0}{2}$$

The algorithm outputs u(i), α_P(i) and α_T(i).

15. The Mie core algorithm

The L2B Mie core algorithm is a Fortran implementation of the L1B Mie core algorithm Option-2 (“Downhill-simplex”), which is defined in Section 15.2 of [RD3].

16. Rayleigh channel error processing

The baseline L2B Rayleigh hlos error quantifier is given in Section 16.2.

An alternative, based on the approach taken for L1B error quantifiers, is retained as an option (Section 16.1).

An error quantifier defined in Section 16.2 requires further minor improvement. The details given in Section 16.2 are only for the error quantifier pertaining to the ILIAD HLOS wind estimate (Sections 12.1 and 12.2). Further details are required for the post-ILIAD terms (Sections 12.3 and 12.4).

16.1. Option for L2B Rayleigh error quantifier based on the L1B approach

Inputs:

RRSR - Rayleigh response sensitivity factor, reported in L1B products

Ka_2, Ka_3, Kb_2, Kb_3 - error quantifier parameters, reported in L1B products

Am(i,k), Bm(i,k) - Measurement Useful Signal in channels A and B, reported in L1B products

λ_0 laser wavelength, reported in L1B products

φ elevation angle, reported in L1B products

W(i,k) - weights, output from Weighting (Section 9)

Outputs:

EQR(i) - L2B Rayleigh error quantifier

The option based on the L1B approach consists of adapting the Error Quantifier approach detailed in section 13.1.3 of L1B DPM (version 1.2 dated 29 September 2005). This approach consists in relating the error estimate to the Rayleigh useful signal M(i) by using the generic function (equation (78))

$$EQRa(i) = \frac{(A(i) + Ka_2)^{Ka_3}}{A(i)}$$

$$EQRb(i) = \frac{(B(i) + Kb_2)^{Kb_3}}{B(i)} \qquad (78)$$

$$EQR(i) = \frac{\lambda_0}{2\sin(\varphi)} \frac{1}{RRSR} \sqrt{EQRa(i)^2 + EQRb(i)^2}$$

Here, the index designates the height bin and Ka_2, Ka_3, Kb_2, and Kb_3, are coefficients determined empirically - stored in the Auxiliary Satellite Characterization Auxiliary and repeated in L1B products.

The use of this equation for the L2B processor is possible, taking into account the definition of meteorologically-weighted useful signal for channels A and B (Section 12.1). Accordingly, equation (77) of the DPM is modified to take into account the variable weight of measurements in the profile

$$A(i) = \frac{\sum_k W(i,k) A_m(i,k)}{\sum_k W(i,k)} \tag{77a}$$

$$B(i) = \frac{\sum_k W(i,k) B_m(i,k)}{\sum_k W(i,k)} \tag{77b}$$

Equation (78) is applied with λ_0=355nm is the laser wavelength and φ is the elevation angle (at height bin level).

The problem is that the parameters Ka_2, Ka_3, Kb_2, and Kb_3, are not known, they shall be established during a pre-launch, on-ground characterization of the instrument. Default values can be found in the Satellite Characterization files delivered with the L1Bp, but may be meaningless.

16.2. Baseline for the ILIAD HLOS error estimate

Inputs:

A_i, B_i - Measurement Useful Signal in Channels A and B, reported in L1B products

$SNR(A_i)$, $SNR(B_i)$ - Measurement SNR in Channels A and B, reported in L1B products

λ_0 laser wavelength, reported in L1B products

φ elevation angle, reported in L1B products

W(i,k) - weights, output from Weighting (Section 9)

$\partial LOS^0 / \partial T$, $\partial LOS^0 / \partial p$, $\partial LOS^0 / \partial R$, $\partial LOS^0 / \partial \rho$ - local derivatives of LOS^0, auxiliary outputs from ILIAD (Section 12.2/14)

σ_T and σ_p - error estimates for Tref and Pref, reported in AUX_MET products

σ_ρ - error estimate for scattering ratio - source TBD, awaiting input from KNMI

Outputs:

EQR(i) - L2B Rayleigh error quantifier

The HLOS error from the ILIAD scheme can be estimated from the SNR of the useful Rayleigh responses A and B, the consequent error in the response $R = (A - B) / (A + B)$, the ILIAD scheme that computes the LOS from R, and the projection of the LOS onto the horizontal.

From a sensitivity analysis it follows that the error in R is

$$\Delta R = \frac{\partial R}{\partial A}\Delta A + \frac{\partial R}{\partial B}\Delta B = \frac{2B}{(A+B)^2}\Delta A + \frac{-2A}{(A+B)^2}\Delta B$$

where A_k and B_k are available on measurement level (L1B DPM section 15-3), and expected standard deviations for ΔA and ΔB, σ_A and σ_B respectively, follow from the signal-to-noise ratio, SNR, respectively $\sigma_{A,k} = A_k / SNR(A_k)$ and $\sigma_{B,k} = B_k / SNR(B_k)$, with k the measurement index.

Note that A_k and B_k may be negative due to the background subtraction (small risk and resulting (high) winds doubtful). As such, it would have been better to request the estimated error standard deviations from L1B at measurement level, rather than the SNR, for the above equation. Now the

L2BP needs to check A_k, B_k, SNR_k < epsilon for precaution. This is implemented in the screening function.

To obtain L2B observations for A and B, A_k and respectively B_k are accumulated over N measurements in a weighted sum, where each of the measurements has a fractional weight $w(i,k)$ (Section 12.1). σ_A and σ_B, on L2B observation level, are thus as well obtained from a weighted sum, respectively

$$\sigma_A^2 = \sum_{k=1}^{N} W(i,k)^2 \sigma_{A,k}^2 \quad \sigma_B^2 = \sum_{k=1}^{N} W(i,k)^2 \sigma_{B,k}^2$$

This computation logically fits in with the other weighting computations (i.e., for A and B) in the code, and not at HLOS error computation level. The SNRs on measurement level will be available from the recent additions to the L1B IODD.

For independent errors in A and B the estimated error in the response R , $\sigma_R = \sqrt{<\Delta R\ \Delta R>}$ with <> the operator for the expected covariance, is obtained by

$$\sigma_R = \frac{2}{(A+B)^2}\sqrt{B^2\sigma_A^2 + A^2\sigma_B^2}$$

This is the first step in the HLOS error computation.

The ILIAD scheme computes in the inversion step the radial wind, LOS^0, from response R , temperature T and pressure p , using the sensitivity $\partial LOS^0 / \partial R$, for a zero scattering ratio, $\rho = 0$. For the given scatter ratio, $\rho \neq 0$, a linear correction is applied

$$LOS = LOS^0 + \rho \frac{\partial LOS^0}{\partial \rho}$$

As such the error is

$$\Delta LOS = \frac{\partial LOS^0}{\partial R}\Delta R + \frac{\partial LOS^0}{\partial T}\Delta T + \frac{\partial LOS^0}{\partial p}\Delta p + \rho\frac{\partial LOS^0}{\partial \rho}$$

where $\partial LOS^0 / \partial T$ and $\partial LOS^0 / \partial p$ are the local sensitivities of the LOS^0 to T and p respectively. For uncorrelated errors in the backscatter ratio, temperature, pressure and the response, the resulting LOS error, $\sigma_{LOS} = \sqrt{<\Delta LOS\ \Delta LOS>}$ with <> the operator for the expected covariance, is estimated as

$$\sigma_{LOS} = \sqrt{\left(\frac{\partial LOS^0}{\partial R}\sigma_R\right)^2 + \left(\frac{\partial LOS^0}{\partial T}\sigma_T\right)^2 + \left(\frac{\partial LOS^0}{\partial p}\sigma_p\right)^2 + \left(\frac{\partial LOS}{\partial \rho}\sigma_\rho\right)^2}$$

$\partial LOS^0 / \partial R$ is about 296 m/s and slightly variable, but is really computed in ILIAD and thus should be exported. $\partial LOS^0 / \partial \rho$ and other sensitivities are available from ILIAD. The terms with the standard deviation of error for temperature and pressure, respectively σ_T and σ_p, are small, but this needs to be further tested. As a start σ_T = 1 K and σ_p = 1 hPa could be taken, but if the temperature and pressure sensitivities are incorporated in the data assimilation system, these values would have to be reset at that point. As such, it may be relevant to report the individual contributions as well in L2B.

In the error budget analysis part of the sensitivity study, KNMI plans to analyse the errors in the diverse backscatter ratio estimates as a first test for the scene classification. For the baseline KNMI suggests to take $\Delta\rho = 0$.

The LOS error in the end needs projection to the horizontal $HLOS$ error by the given projection angle, where the associated projection error is neglected (order 0.01 m/s if properly specified):

$$\sigma_{HLOS} = \frac{\lambda_0}{2\sin(\varphi)}\sigma_{LOS}$$

17. Mie channel error processing

The baseline L2B Mie hlos error quantifier is given in Section 17.2.

An alternative definition, based on the approach taken for L1B error quantifiers, is retained as an option (Section 17.1).

17.1. Option for L2B Mie error quantifier based on L1B approach

Inputs:

K_1, K_2, and K_3 - error quantifier parameters, reported in L1B products

LID(i,j,k) - spectrometer counts, reported in L1B products

λ_0 laser wavelength, reported in L1B products

φ elevation angle, reported in L1B products

W(i,k) - weights, output from Weighting (Section 9)

Outputs:

EQM(i) - L2B Mie error quantifier

The option based on the L1B approach consists of adapting the Error Quantifier approach detailed in section 13.1.2 of L1B DPM (version 1.2 dated 29 September 2005). This approach consists in relating the error estimate to the Mie useful signal M(i) by using the generic function (equation (74))

$$EQM(i) = \frac{\lambda_0}{2\sin(\varphi)} K_1 \frac{(M(i) + K_2)^{K_3}}{M(i)}$$

Here, the index designates the height bin and K_1, K_2, and K_3 are coefficients determined empirically - stored in the Auxiliary Satellite Characterization Auxiliary and repeated in L1B products.

The use of this equation for the L2B processor is possible. The algorithm would be start with the removal of the offset read-out offset

$$\mathrm{LID(i,j,k)} = \mathrm{LID(i,j,k)} - \frac{1}{2}\sum_{j=19}^{20} \mathrm{LID(i,j,k)} \quad (70)$$

Then the background is removed

$$\mathrm{LID(i,j,k)} = \left[\mathrm{LID(i,j,k)} - \frac{t_i}{t_i'} \mathrm{LID(25,j,k)} \right] \quad (71)$$

Equation (72) of the DPM is modified to take into account the variable weight of measurements in the profile

$$LID(i,j) = \frac{\sum_k W(i,k) LID(i,j,k)}{\sum_k W(i,k)} \qquad (72')$$

The weight-averaged spectra are then integrated to get the useful signal

$$M(i) = \sum_{j=3}^{18} LID(i,j) \qquad (73)$$

and equation (74) is applied with λ_0=355nm is the laser wavelength and φ is the elevation angle (can take 35 degrees for a start or the DEM intersection elevation given in L1B IODD - table 5-14 on page 5-9, and later the elevation angle at height bin level).

The problem is that the parameters K_1, K_2 and K_3 are not known, they shall be established during a pre-launch, on-ground characterization of the instrument. Default values can be found in the Satellite Characterization files delivered with the L1Bp, but may be meaningless.

17.2. Baseline for L2B Mie error quantifier

Note: the definition in this section is provisional and subject to future improvement.
In particular, additional terms are needed for contributions from internal reference and from post-core correction terms (see Section 13).

Inputs:

LID(i,j,k) - spectrometer counts, reported in L1B products

$T_{obs}(j)$ - tripod obscuration factors, reported in L1B products

λ_0 laser wavelength, reported in L1B products

φ elevation angle, reported in L1B products

W(i,k) - weights, output from Weighting (Section 9)

peak_height, $FWHM$ and $\hat{f}_{mie}$ (in frequency units) - outputs of the Mie core algorithm (Section 13.2

USR: useful spectral range, reported in L1B products or set as a configuration parameter (TBD)

Outputs:

EQM(i) - L2B Mie error quantifier

The baseline for the L2B Mie error quantifier is the error standard deviation given by the equation:

$$EQM(i) = \frac{\lambda_0}{2\sin\varphi}\left[\sum_{j=3}^{18}\alpha(i,j)^2\right]^{-1}\sqrt{\sum_{j=3}^{18}\sigma_{i,j}^2\alpha(i,j)^2} \qquad (74)$$

where

$$\sigma_{i,j}^2 = \sum_{k=1} W^2(i,k) LID(i,j,k) \qquad (75)$$

is an estimate for the variance of the weighted sum of photo-counts $\mathrm{LID}(i,j,k)$ (from equation (71), that is, after removal of the video offset), $W(i,k)$ is the weight associated to bin i, measurement k for the profile at stake, and

$$\alpha(i,j) = T_{obs}(j)\ \mathrm{peak\_height}\left[\frac{1}{1+\frac{4\left(f_j^{+}-\hat{f}_{mie}(i)\right)}{FWHM^2}}-\frac{1}{1+\frac{4\left(f_j^{-}-\hat{f}_{mie}(i)\right)}{FWHM^2}}\right] \tag{76}$$

Here, $\mathrm{peak\_height}$, FWHM and $\hat{f}_{mie}$ (in frequency units) are the outputs of the Mie core algorithm (peak height and FWHM of the fitted Lorentzian spectrum, and Mie frequency estimate), $T_{obs}(j)$ is the tripod obscuration factor for CCD bin j, and $f_j^{+,-}$ are the upper and lower frequencies of CCD bin j:

$$f_j^{-} = (j-3)\frac{USR}{16}-\frac{USR}{2} \quad \text{and} \quad f_j^{+} = (j-2)\frac{USR}{16}-\frac{USR}{2} \tag{77}$$

(USR=1500 MHz).

18. Retrieval of atmospheric optical properties

The retrieval of atmospheric optical properties by the L2B processor is controlled by processing parameters in the AUX_PAR_2B input file. The algorithms that can be selected by appropriate parameter settings are as follows.

The algorithms presented in this section estimate atmosphere optical parameters from measured data in the Mie and/or Rayleigh channels and auxiliary NWP data. More specific, procedures to estimate profiles of particle and molecular backscatter, extinction, optical thickness, transmission and backscatter-to-extinction ratio are described.

Output parameters for each bin are particle optical thickness and the scattering ratio. Particle optical thickness is used for scene classification as discussed in section 7. The scattering ratio is an important parameter in the ILIAD scheme to correct derived Rayleigh winds for Mie contamination in the Rayleigh channel signal.

18.1. Estimation of atmosphere optical properties using the Rayleigh channel only

Depending on the vertical sampling strategy, but at least for the top couple of bins no Mie but only the Rayleigh signal will be available. The objective in this section is to estimate particle optical thickness within a range gate from the Rayleigh channel signal only.

18.1.1. Input parameters

The input parameters needed to determine the particle optical thickness and scattering ratio within a range gate are

1. S_{ray} (i): the measured Rayleigh signal in the range bin, from L1B;
2. R_i: the range from the atmospheric bin to the satellite from L1B;
3. the bin size Δz from L1B;
4. K_{ray}, C_1(i): Rayleigh channel calibration value
5. $\beta^M(z)$ and $\tau^M(z)$: Rayleigh backscatter and transmission from NWP data, Eq. (C19).
6. Thresholds

18.1.2. Output parameters

1. α_i^p: particle extinction within range bin *i*
2. ρ_i: scattering ratio within range bin *i*
3. $\partial\rho/\partial\kappa^P$: Sensitivity of the scattering ratio estimate to uncertainty in the value for the particle backscatter-to-extinction ratio κ^P (sr^{-1})
4. σ_ρ: Standard deviation of error in the estimate for ρ
5. Flags

18.1.3. Algorithm

Discrimination between two types of particles is considered:

1. background aerosol that is present in each range bin but optically thin
2. a layer of particles (either aerosol or cloud) that can be distinguished from the background aerosol.

The algorithm to compute aerosol transmission from the measured FP signal is outlined in Appendix E.

In case of a particle layer substantial contamination of the FP channel signal is expected through cross-talk. The layer is detected by comparing the measured and expected signal for the bin under investigation, the latter signal assuming no particles. In case of no particle layer, the measured signal will always be smaller than the expected signal due to aerosol transmission. In case of a particle layer, the measured signal may be larger than the expected signal if the signal increase through cross-talk exceeds the signal loss due to transmission. The 2-way transmission of the particle layer, $(\tau^{\text{layer}})^2(i)$, is obtained from the quotient of the measured and expected (assuming no particles in the bins covering the layer) FP signals below the cloud. The expected signal, $\hat{S}_{\text{FP}}(i)$, in bin *i*, is obtained by assuming no particles in bin *i*, (dashed line in Figure A) and is estimated from Eq.(C16), with $C = C_1$, since $\rho = 1$:

$$\hat{S}_{\text{FP}}(i) = K_{\text{ray}} C_1(v,P,T)\beta^{\text{M}}(i)\frac{\Delta z_i}{R_i^2}\prod_{j=0}^{i-1}\left[\tau^{\text{P}}(j)\tau^{\text{M}}(j)\right]^2\tau^{\text{M}}(i) \qquad \textbf{Eq. 18.1}$$

If there *are* particles in bin *i* then the measured signal, $S_{\text{FP}}(i)$, in bin *i* (solid line in Figure A) will be different from expectation due to particle backscatter (gain) and transmission (losses). The balance of losses and gains will be further tested. Assuming mainly losses we find for $\tau^{\text{layer}}(i)$:

$$\tau^{\text{layer}}(i) = \sqrt{\frac{S_{\text{FP}}(i)}{\hat{S}_{\text{FP}}(i)}}, \quad \alpha^{\text{layer}}(i) = -\frac{\cos(\hat{\theta})\ln(\tau^{\text{layer}}(i))}{\Delta z_i}, \quad \delta^{\text{layer}}(i) = -\cos(\hat{\theta})\ln(\tau^{\text{layer}}(i)) \qquad \textbf{Eq. 18.2}$$

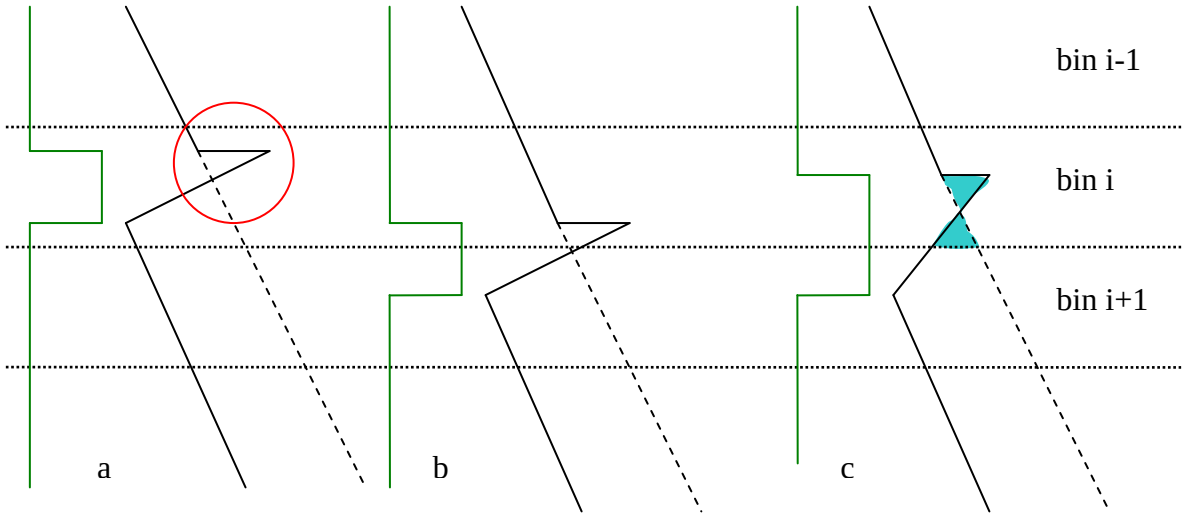

Figure A. Atmosphere particle backscatter layer (green) and return signal detected by the Rayleigh channel (black solid line) a) in case of a layer with a uniform particle distribution (aerosol or cloud) in bin i or b/c) in case that the layer extends over 2 bins. The dashed lines denotes the "expected" signal in the absence of the particle layer. The peak in the red circle is the result of contamination of particles in the Rayleigh channel (cross-talk). See text for further details.

In case of a particle free bin, the value for particle transmission, τ^{layer}, in the troposphere and stratosphere will be close to 1. Figure A shows a number of possible situations for particle layers. Figure Aa depicts the simplest case where the particle layer lies completely within one bin. Generally the extinction losses will be larger than the backscatter gain (through cross-talk), thus yielding a value for τ^{layer} smaller than 1 that can be detected by a threshold value, τ_{low} smaller than 1, below the particle layer.

In case the top particle layer may present more backscatter gain than extinction losses e.g. if the top of the layer is positioned at the bottom of the bin and the layer extends over more than 1 bin, see Figure Ab, then τ^{layer} is larger than 1 (and thus giving negative extinction). This can be detected by a threshold, τ_{up} larger than 1.

Range gates with particle transmission larger than τ_{up} or smaller than τ_{low} will be flagged as suspicious for Rayleigh retrieval. To be conservative, the next range bin above the highest flagged range gate is also flagged suspicious. This is motivated by the case depicted in Figure Ac where the layer extends over two bins and signal losses through extinction in bin *i* is fully compensated by signal gain through cross-talk (equal surface of the blue triangles). This yields a transmission value of 1 despite the presence of particles.

The result of the above algorithm for the scenes in Figure A yields

- Scene a: bins i-1, and i are flagged
- Scene b: bins i and i+1 are flagged
- Scene c: bins i and i+1 are flagged

The number of cases in the stratosphere and upper troposphere with particle contamination in subsequent range gates, where only the Rayleigh channel is available, will be verified in the sensitivity study. As such, a more sophisticated algorithm may emerge.

Checks are implemented, e.g. to test for unrealsitic negative values of S_{ray}, $\hat{S}_{ray}$ and τ_i^P e.g. due to measurement noise or values for τ_i^P exceeding 1. The accuracy of the estimated particle transmission and subsequent optical depth are assessed as a function of the quality of NWP input data in the sensitivity study.

The transmission of the particle layer is determined by dividing the expected (no particles) and measured signals below the particle layer. The layer transmission is included in the computation of the expected signal to detect eventually layers further down in the profile.

18.2. Scattering ratio estimation using the Rayleigh channel only

Scattering ratio is an important parameter in the processing to derive HLOS wind estimates from the Rayleigh channel signal to correct for the contamination of the Mie signal into the Rayleigh channel (ref, ILIAD).

18.2.1. Input parameters

The input parameters needed to determine the scattering ratio within a range gate are

1. δ_i^p: particle optical depth, from section 6.1.3.
2. β^M: Rayleigh backscatter from NWP data, Eq. (C19).
3. A priori knowledge of the particle backscatter-to-extinction ratio κ^P (sr^{-1}) profile, e.g. from global statistics of κ^P as a function of latitude and height. Here we assume that values for the mean and standard deviation, σ_κ^p, of κ^P are known over the globe.

18.2.2. Output parameters

1. ρ : scattering ratio.
2. $\partial\rho/\partial\kappa^P$: Sensitivity of the scattering ratio estimate to uncertainty in the value for the particle backscatter-to-extinction ratio κ^P (sr^{-1})
3. σ_ρ: Standard deviation of error in the estimate for ρ

18.2.3. Algorithm

Particle backscatter and extinction may be related through a particle backscatter-to-extinction ratio κ^P (sr^{-1}), that may depend on the altitude *z*, since different atmospheric layers may constitute different types of aerosol:

$$\beta_i^P = \kappa_i^P \alpha_i^P \qquad \textbf{Eq. 18.3}$$

Assuming a known particle backscatter-to-extinction ratio κ_i^P (sr^{-1}) for particles in the *i*-th bin, the particle backscatter is obtained directly from Eqs. (18.2),(18.3). The scattering ratio then follows from Eq. (C17)

The scattering ratio is an important parameter in the ILIAD correction scheme for the reliability of derived Rayleigh winds. Uncertainty in κ_i^P and subsequent estimate of the scattering ratio induces an error in the derived Rayleigh wind. The sensitivity of the estimated scattering ratio to uncertainty in κ^P is obtained through

$$\frac{\partial \rho}{\partial \kappa^p} = \frac{1}{\beta^M}\frac{\partial \beta^P}{\partial \kappa^p} = \frac{\alpha_i^P}{\beta_m} \qquad \textbf{Eq. 18.4}$$

A first oder estimate of the error in ρ then equals $\Delta\rho = \partial\rho/\partial\kappa^P \Delta\kappa^P$, and thus for the standard deviation of error in ρ:

$$\sigma_\rho = \frac{\alpha^p}{\beta_m}\sigma_{\kappa_p} \qquad \textbf{Eq. 18.5}$$

This parameter will be quantified in the sensitivity study.

18.3. Estimation of atmosphere optical properties using the Mie channel only

In case that only the signal from the Mie channel is available (lower atmosphere with large particle optical thickness, no/incorrect calibration of the Rayleigh channel, Rayleigh channel out of order, etc), the particle optical thickness may be determined from the Mie channel signal only.

18.3.1. Input parameters

1. ρ : scattering ratio from L1B
2. Atmospheric pressure and temperature from the auxiliary meteorological data
3. β^M: molecular backscatter from NWP data, Eq. (C19)
4. κ^p: particle backscatter-to-extinction ratio (sr^{-1})

18.3.2. Output parameters

1. δ^p: particle optical thickness
2. ρ: scattering ratio

18.3.3. Algorithm

Particle backscatter is obtained from the scattering ratio and molecular backscatter using a rearrangement of Eqs.(C17,C19). Next, particle extinction follows from Eq.(18.3). This requires a priori knowledge of the particle backscatter-to-extinction ratio. Then optical thickness follows from the relationship $\delta^P = \alpha^P \Delta z$.

Note. The main parameter for scene classification is particle optical thickness. The quality of its estimate from the algorithm above depends on the a priori knowledge of the particle backscatter-to-extinction ratio that is related to atmospheric flow and may vary substantially with climate zone and altitude. Therefore, the quality of the L1B scattering ratio will also be tested for use in scene classification in the sensitivity study in addition to using particle optical thickness. Moreover, extinction may be estimated from the knowledge of the NWP molecular backscatter and the Rayleigh backscatter estimate from the offset parameter of the Mie core algorithm. The potential for this needs to be tested.

18.4. Estimation of atmosphere optical properties using both the Mie and Rayleigh channels

In nominal mode, in the troposphere, both the Mie and Rayleigh channel signals are available. Then, at least two options are available to estimate the scattering ratio for the Rayleigh bin:

1 Directly from L1Bp. In case that more than one Mie bin falls within a Rayleigh bin, the scattering ratio for each sub-bin is obtained from L1B. The Rayleigh bin scattering ratio is obtained from the average of the sub-bins values.
2 From the measured Rayleigh and Mie signals directly without additional prior knowledge of the atmosphere.

The second option is further discussed here. Using Eqs (C16,C18), and using the scattering ratio definition Eq (C17), the ratio of the Rayleigh and Mie channel signals equals

$$\frac{S_{\mathrm{ray}}(i)}{S_{\mathrm{mie}}(i)+N_{\mathrm{mie}}(i)} = \frac{K_{\mathrm{ray}}\left[C_1(i)+C_2(i)(\rho_i-1)\right]\beta_i^M \frac{\Delta z_i}{R_i^2}\prod_{j=0}^{i-1}\left[\tau_j^P\tau_j^M\right]^2\tau_i^P\tau_i^M}{K_{\mathrm{mie}}\left[C_4(i)+C_3(i)(\rho_i-1)\right]\beta_i^M \frac{\Delta z_i}{R_i^2}\prod_{j=0}^{i-1}\left[\tau_j^P\tau_j^M\right]^2\tau_i^P\tau_i^M} = \frac{K_{\mathrm{ray}}\left[C_1(i)+C_2(i)(\rho_i-1)\right]}{K_{\mathrm{mie}}\left[C_4(i)+C_3(i)(\rho_i-1)\right]}$$

hence

$$\rho_i = 1+\frac{\lambda_i C_4(i)-C_1(i)}{C_2(i)-\lambda_i C_3(i)}, \qquad \lambda_i = \frac{K_{\mathrm{mie}}S_{\mathrm{ray}}(i)}{K_{\mathrm{ray}}\left[S_{\mathrm{mie}}(i)+N_{\mathrm{mie}}(i)\right]} \qquad \textbf{Eq. 18.6}$$

Note. In case that more than one Mie bin falls within a Rayleigh bin, the Mie sub-bin signals are accumulated before the computation above is performed.

Checks will be implemented to test for unrealistic values of the scattering ratio, e.g. smaller than 1.

Both options will be tested in the sensitivity study, starting with the first option. It is noted that the sub-bin Mie information is required for correct height assignment of Rayleigh winds in case of substantial extinction within a range gate.

18.4.1. Input parameters

1. ρ_i: scattering ratio from L1B or Eq.(18.6);
2. β_i^M and τ_i^M: Rayleigh backscatter and transmission from NWP data, Eq. (C19);
3. Rayleigh channel calibration constants K_{ray}, $C_1(i)$, $C_2(i)$;
4. C_3, C_4, K_{mie}, N_{mie}, S_{ray}, S_{mie};

18.4.2. Output parameters

1. δ_i^P: particle optical thickness
2. κ_i^P: particle backscatter-to-extinction ratio (sr^{-1})

18.4.3. Algorithm

Particle optical thickness is computed from Rayleigh signal extinction similar as in section 6.1. For the expected signal, $\hat{S}$, a better estimate is obtained by using $C=C_1+C_2(\rho_i-1)$ instead of C_1 into Eq.(18.1), since an estimate for ρ_i is available here. Particle optical thickness then follows from Eq.(18.2):

Similar checks as in the previous sections are implemented to test the realism of the computed atmosphere optical parameters.

In addition, an estimate of the backscatter-to-extinction ratio is obtained from (see Eqs.(18.2),(18.3)):

$$\kappa_i^P = \frac{\beta_i^P \Delta z_i}{\delta_i^P} \qquad \textbf{Eq. 18.7}$$

The estimated backscatter-to-extinction ratio is verified against the climatology as a function of zone and height. (In addition, the climatology may be updated by such operation off-line.)

Note that the quality of all estimated atmosphere optical parameters is contaminated with measurement noise. More sophisticated (noise reducing, maximum likelihood) algorithms are needed for low SNR measurements. This may be investigated in the sensitivity study.

19. Matchup

Given the L1B measurement locations for a particular BRC, and a set of auxiliary meteorological data available at reference locations, the purpose of the matchup algorithm is to obtain a selected subset of auxiliary meteorological data profiles, to provide the closest match to the L1B measurement locations.

The auxiliary meteorological data provided to the L2BP (e.g. in AUX_MET_12 files) consist of a large set of profiles (and associated surface values). In general, the reference locations at which the meterological profiles are given are close to the Aeolus measurement positions, but a one-to-one correspondence cannot be guaranteed. During the preprocessing step (see Appendix A.2) that generated the reference meteorological data, the locations may already have been interpolated to the exact BRC locations, but this is not a requirement. Even if an interpolation is done, only for the center of the BRC the profile matches exactly.

Auxiliary meteorological data may also be offered to the L2BP at the closest grid positions available in the NWP model, or at regular (50 km interval) positions along a predicted ground track.

This means that the L2BP needs some algorithm to choose which meteorological profile to use, and if needed interpolate between a set of nearby NWP profiles. Note that Met centers may implement their own algorithm to enable for example interpolation between NWP profiles, in case use of high resolution data is desired. The L2BP provides for two simple algorithms to be used here.

Inputs:

- L1B geolocation for one BRC (lat,lon,date,time for each measurement)
- an array of NWP profiles and associated lat,lon,date,time for each reference profile
- Thresholds on the allowed distance range and time window (from L2B Aux Par file)

Outputs:

- the index of the selected NWP profile

Algorithm:

Currently two matching algorithms have been implemented:

- Dummy Matchup
- Nearest Neighbour Matchup

19.1. Dummy Matchup

The Dummy algorithm does not take any lat,lon or date,time information into account. It assumes that for every BRC an appropriate NWP profile is available, and matches them using the order in which they appear in the input files. The output index is simply the L1B BRC number. So BRC 1 in the L1B file is always combined with NWP profile 1 in the AMD file, BRC 2 in the L1B file is always combined with NWP profile 2 in the AMD file, etc.

19.2. Nearest Neighbour Matchup

The Nearest Neighbour Matchup algorithm consists of the following steps for each BRC:

- calculate the position and time of the center of the BRC
- apply a time window on all available NWP profiles
- apply a distance range check to all NWP profiles
- loop along all NWP profiles that passed the above two checks and choose the profile closest to the BRC center position

No interpolation between NWP profiles is implemented at the moment.
The four steps are implemented as follows:

19.2.1. Calculate BRC center

Inputs:

- lat,lon,date,time of the first and last measurement of this BRC

Outputs:

- lat,lon,date,time of the BRC center

Algorithm:

- convert both lat-lon pairs to (x,y,z) unit vectors

$$x = \cos(\lambda)\cos(\delta)$$
$$y = \sin(\lambda)\cos(\delta)$$
$$z = \sin(\delta)$$

in which latitude δ and longitude λ are given in radians

- do a vector average

$$x_{mid} = (x_1 + x_2)/2$$
$$y_{mid} = (y_1 + y_2)/2$$
$$z_{mid} = (z_1 + z_2)/2$$

- renormalise to 1

$$r_{norm} = \sqrt{x_{mid}^2 + y_{mid}^2 + z_{mid}^2}$$
$$x_{mid} = x_{mid} / r_{norm}$$
$$y_{mid} = y_{mid} / r_{norm}$$
$$z_{mid} = z_{mid} / r_{norm}$$

- convert xyz back to lat,lon

$$\text{if } z \geq 0 : \lambda = +\cos^{-1}\sqrt{x^2 + y^2}$$
$$\text{if } z \geq 0 : \lambda = \cos^{-1}\sqrt{x^2 + y^2}$$
$$\text{if } y = 0 \wedge x = 0 : \lambda = 0$$
$$\text{else } \lambda = \text{atan2}(y, x)$$

in which atan2() is the Fortran90 function that gives a proper angle in the range $-\pi$ to π if x and y are the sides of a right angled triangle.

- calculate the time difference ΔT in seconds between both date,time pairs. d=daynumber, s=seconds since midnight (for convenience seconds are treated as reals, so the microseconds since start of this second have been included in them).

$s_{day} = 24 * 60 * 60 = 86400$ denotes the number of seconds in a day

$$\Delta T = s_{day} * (d2 - d1) + (s2 - s1)$$

- add half the timedifference to date-time pair 1

$$s_{mid} = s_{day} + \Delta T / 2$$
$$\text{if } s_{mid} < 0 : \text{day}_{\text{offset}} = 1 + floor(s_{mid} / s_{day});$$
$$d_{mid} = d_m - \text{d}_{\text{offset}}; s_{mid} = s_{mid} + \text{d}_{\text{offset}} * s_{day}$$
$$\text{if } s_{mid} > s_{day} : \text{d}_{\text{offset}} = floor(s_{mid} / s_{day});$$
$$d_{mid} = d_1 + \text{d}_{\text{offset}}; s_{mid} = s_{mid} - \text{d}_{\text{offset}} * s_{day}$$

19.2.2. Apply timewindow

Inputs:

- date and time of the BRC center and of the current NWP profile
- Max_Allowed_Time_Diff $\Delta T_{\max}$ from L2B_Aux_Par

Outputs:

- decision: in timewindow or not

Algorithm:

- calculate the time difference in seconds between both date,time pairs

$$\Delta T = s_{day} * (d2 - d1) + (s2 - s1)$$

- if $\Delta T < \Delta T_{\max}$ then this NWP profile may be used

19.2.3. Apply a distance range

Inputs:

- lat,lon of the BRC center and of the current NWP profile
- Max_Allowed_Distance $D_{\max}$ from L2B_Aux_Par

Outputs:

- profile within range or not

Algorithm:

- convert both lat,lon pairs to (x,y,z) unit vectors

$$x = \cos(\lambda)\cos(\delta)$$
$$y = \sin(\lambda)\cos(\delta)$$
$$z = \sin(\delta)$$

- calculate the angle between both vectors α in radians, assuming the earth is a perfect globe using the goniometric property that the inner product between two unit vectors equals the cosine of the angle between them

$$\alpha = \text{acos}(x1 * x2 + y1 * y2 + z1 * z2)$$

- convert the angle distance α to a surface distance D in km, using the earths radius R in km: $D = R * \alpha$. We use the equatorial earth radius $R_{eq} = 6378.1$ km
- if $D \le D_{\max}$ then this NWP profile may be used

19.2.4. Choose closest NWP profile

Inputs:

- lat,lon of the BRC center and of the allowed set of NWP profiles that passed the distance range and timewindow tests

Output:

- index of the selected NWP profile

Algorithm:

- Calculate the distance (as described above) between the BRC center and each allowed NWP profile in a loop and select the NWP profile closest to the BRC center position. Then report its index.

Appendix A. Auxiliary processing

This appendix describes auxiliary processing, i.e. provision of auxiliary meteorological data, as performed at the operational Level-2B processing facility (i.e. ECMWF.) Other meteorological centres will adapt the processing described here to suit their own needs. For further guidance see [RD6].

A.1. Determine reference locations for computing auxiliary meteorological data

Inputs:

- L1B geolocation information (latitude, longitude, time) for each measurement and observation. As a minimum, the geolocation of the intersection of the DEM and the line-of-sight, applicable for the observation centroid (L1B tags “Geolocation_of_DEM_Intersection” and “Observation_Centroid_Time”).
- Predicted flight track information: orbit prediction vectors delivered from the Core PDS to ECMWF in the form of one delivery of state vectors per 24 hours, each covering a period of 7 days (109 orbits) ahead. The most recent predictions are used.

Outputs:

- Reference locations (latitudes, longitudes and times) for computation of auxiliary meteorological data

Algorithm:

- For each valid L1B dataset record received in time for nominal NRT/QRT processing, a reference location (latitude, longitude, time) is selected, at which auxiliary meteorological data are to be computed. In operational mode, the reference location is the DEM intersection, applicable for the observation centroid, as specified in L1B data. The meteorological data are to take the form of vertical profiles at each reference location, together with any model information (details of vertical and/or horizontal grid structure) that may be required to facilitate collocation to L1B measurement locations, prior to selective weighting (including interpolation to requested locations as a special case) within primary L2B processing (Secs 5.3/5.4). In operational mode the auxiliary data validity time may differ by up to 15 minutes from the data acquisition time of the L1B input. At other meteorological centres, the selection of suitable reference locations may be driven either by the geolocation information of L1B data or by the available meteorological model. Precise details will depend on the particular implementation of L2B processing at different sites.
- (Operational mode only.) Reference locations are also selected for the predicted flight track of each orbit. Using the EE CFI and an orbit prediction utility supplied by ESA, predicted flight tracks are computed for both the sub-satellite track (nadir-pointing) and nominal (35 degrees off-nadir) configurations of the Aeolus satellite. The along-track spacing between such locations is currently set to 50 km. The inputs are orbit prediction vectors provided by the Core PDS to ECMWF, one delivery of state vectors per 24 hours, each covering a period of 7 days (109 orbits) ahead.

- (Operational mode only.) The locations determined by i) and ii) are merged. The merge sub-task is achieved automatically through integration of the L2B processor with the ECMWF data assimilation system, ie inside ECMWF's Observation DataBase (ODB)

A.2. Generate auxiliary meteorological data at reference locations

Description:

i. At each reference location (input), compute the auxiliary meteorological data required for collocation to L1B measurement locations and subsequent HLOS retrieval (Table 4.1/4.2). The data to be computed also anticipate meteorological parameters (related to humidity and cloud) that are not required for L2B processing but which may be useful in L2A processing. In operational mode, the data will be vertical profiles (not slanted), and their computation will occur as a consequence of integrating Aeolus processing with ECMWF's existing processing of meteorological observations. Collocation to L1B measurement locations occurs in a separate task ("pre-processing", Item 5.3). Use of geoid height data is deferred to Items 5.3/5.4. Selection of the reference locations supplied as input is explained in Section 5.1. Consequently, such selection may be driven either by the geolocation information of L1B data, by predicted ground track information, or by the available meteorological model. Precise details will depend on the particular implementation of L2B processing at different sites,

Inputs:

- Reference locations (latitude, longitude, time) for computation of auxiliary meteorological data
- Meteorological fields

Outputs:

- Meteorological profile data at reference locations, i.e. prior to pre-processing (Table 4.1/4.2). The vertical coordinates of the meteorological input are retained.

Algorithm:

- The task is achieved through integration of the L2B processor with the ECMWF data assimilation system. A standard part of the system, known as screening job, involves 1) the computation of background meteorological fields, and 2) interpolation in space and time to the location of meteorological observations. The background fields are obtained from a short-term forecast initialized with the meteorological analysis from the previous assimilation window.
- By treating Aeolus data as meteorological observations, the meteorological profile data needed for Aeolus processing are obtained.

A.3. Pre-process auxiliary meteorological data

Preprocessing of auxiliary meteorological data involves transformations from raw auxiliary meteorological profile to the measurement scale of L1B data. In the operational L2B processor only one raw profile is available per BRC. In this case, pre-processing consists of extrapolation:

$$f_m = f_{raw}, \quad m = 1, \ldots, N$$

Appendix B. Mie error quantifier derivation

This appendix clarifies the assumptions, and provides details of the mathematics, that lead to the expression proposed in Section 17.2 for predicting the level of error on Mie winds.

The Mie core algorithm estimates the frequency of the Mie return by minimizing the cost function:

$$J(f)=\sum_{j=3}^{18}\left[N(i,j)-\mu_j(f)\right]^2 \tag{B1}$$

where $N(i,j)$ is a weighted photo-count for i-th height-bin and j-th CCD bin and $\mu_j(f)$ is a prediction of the same number based on an ad-hoc model (at present, a Lorentzian on top a uniform level of background light).

The photo-counts $N(i,j)$ are computed from the measurement level CCD photo-counts $LID(i,j,k)$ (after the removal of the video offset):

$$N(i,j)=\sum_{k=1}^{N_{meas}} w_k LID(i,j,k) \tag{B2}$$

where N_{meas} is the total number of measurements and w_k are the weights allocated to measurement k.

In equation (B1), the minimization bears only on the frequency, while 4 parameters are optimized by the Mie core algorithm (the central frequency, the amplitude, the width and the uniform level of background light). Here, we simplify the problem by limiting the optimization to the single frequency parameter, hoping that the equation we derive will apply with no major deficiency to the more complex case.

Let us denote by f_0 the frequency that optimizes the cost function

$$\bar{J}(f)=\sum_{j=3}^{18}\left[\bar{N}(i,j)-\mu_j(f)\right]^2 \tag{B3}$$

where $\bar{N}(i,j)$ denotes the mathematical expectation of N_j. Then, let us approximate $J(f)$ around f_0 by a second order expansion:

$$J(f)\approx J(f_0)+\frac{\partial J}{\partial f}(f-f_0)+\frac{1}{2}\frac{\partial^2 J}{\partial f^2}(f_0)(f-f_0)^2 \tag{B4}$$

and assume that the frequency $\hat{f}$ that minimizes $J(f)$ is very close the frequency that minimizes (B3). This assumption can be written:

$$\hat{f}\approx f_0-\left[\frac{\partial^2 J}{\partial f^2}(f_0)\right]^{-1}\frac{\partial J}{\partial f}(f_0) \tag{B5}$$

Now, let us denote $J'(f)=J(f)-\bar{J}(f)$ and assume

$$\frac{\partial J'}{\partial f}(f_0)<<\frac{\partial \bar{J}}{\partial f}(f_0)\ \text{and}\ \frac{\partial^2 J'}{\partial f^2}(f_0)<<\frac{\partial^2 \bar{J}}{\partial f^2}(f_0) \tag{B6}$$

Equation (B4) can then be approximated by the first order expansion

$$\hat{f} - f_0 \approx -\left[\frac{\partial^2 \bar{J}}{\partial f^2}(f_0)\right]^{-1}\left[\frac{\partial \bar{J}}{\partial f}(f_0) + \frac{\partial J'}{\partial f}(f_0)\right] = -\left[\frac{\partial^2 \bar{J}}{\partial f^2}(f_0)\right]^{-1}\frac{\partial J'}{\partial f}(f_0) \quad \text{(B7)}$$

From which follows that

$$\left\langle \left(\hat{f} - f_0\right)^2 \right\rangle = \left[\frac{\partial \bar{J}}{\partial f}(f_0)\right]^{-2}\left\langle \frac{\partial J'}{\partial f}(f_0)\frac{\partial J'}{\partial f}(f_0)\right\rangle \quad \text{(B8)}$$

From (B1) and (B3), we can write

$$J'(f) = \sum_{j=3}^{18} N'(i,j)^2 - 2\sum_{j=3}^{18} N'(i,j)\left[\bar{N}(i,j) - \mu_j(f)\right] \quad \text{(B9)}$$

so

$$\frac{\partial J'}{\partial f}(f_0) = 2\sum_{j=3}^{18} N'(i,j)\alpha_j(f_0) \quad \text{(B10)}$$

where $\alpha_j(f_0) = \partial\mu_j(f_0)/\partial f$. Since $\left\langle N'(i,j)N'(i,k)\right\rangle = \sigma_{i,j}^2\,\delta(j-k)$ (the random fluctuations of the photo counts are independent), it follows that

$$\left\langle \frac{\partial J'}{\partial f}(f_0)\frac{\partial J'}{\partial f}(f_0)\right\rangle = 4\sum_{j=3}^{18}\sigma_{i,j}^2\alpha_j^2 \quad \text{(B11)}$$

From equation (B3)

$$\frac{\partial^2 \bar{J}}{\partial f^2}(f_0) = -2\sum_{j=3}^{18}\frac{\partial \alpha_j}{\partial f}(f_0)\left[\bar{N}(i,j) - \mu_j(f_0)\right] + 2\sum_{j=3}^{18}\alpha_j^2(f_0) \quad \text{(B12)}$$

The first term can be neglected if $\bar{N}(i,j) \approx \mu_j(f_0)$. This condition should be met as long as the model $\mu_j(f)$ is a good model for the photo-counts $\bar{N}(i,j)$, so we can make the approximation

$$\frac{\partial^2 \bar{J}}{\partial f^2}(f_0) = 2\sum_{j=3}^{18}\alpha_j^2(f_0) \quad \text{(B13)}$$

Now, combining (B11) and (B13) gives

$$\boxed{\left\langle \left(\hat{f} - f_0\right)^2 \right\rangle \approx \left[\sum_{j=3}^{18}\alpha_j^2(f_0)\right]^{-2}\sum_{j=3}^{18}\sigma_{i,j}^2\alpha_j^2(f_0)} \quad \text{(B14)}$$

This is the basis for the expression given in Section 17.2 which uses the photo-count model

$$\mu_j(f) = T_j^{obs}\int_{f_j^-}^{f_j^+}\left[\frac{2A}{\pi\Delta}\left[1 + \frac{4(x-f)^2}{\Delta^2}\right]^{-1} + B\right]dx \quad \text{(B15)}$$

where f_j^+ and f_j^+ are the upper and lower frequency bounds of CCD bin j, T_j^{obs} is the tripod obscuration factor for bin j, Δ is the FWHM of the Lorentzian spectrum assumed for the Mie return, A is its amplitude, and B is the uniform level of background light. Considering this model, it follows that

$$\alpha_j(f_0) = T_j^{obs}\frac{2A}{\pi\Delta}\left[\frac{1}{1+\frac{4\left(f_j^{+}-f_0\right)^2}{\Delta^2}} - \frac{1}{1+\frac{4\left(f_j^{-}-f_0\right)^2}{\Delta^2}}\right] \quad \text{(B16)}$$

In practice, A, Δ and f_0 are approximated with the parameters estimated by the Mie core algorithm, the link between both sets being

$$\begin{aligned} \text{peak\_height} &\leftrightarrow \frac{2A}{\pi\Delta} \\ \text{FWHM} &\leftrightarrow \Delta \\ \text{frequency estimate} &\leftrightarrow f_0 \end{aligned} \quad \text{(B17)}$$

It now remains to give an expression for $\sigma_{i,j}^2$. If we assume that the random fluctuations of $LID(i,j,k)$ follow independent, Poisson statistics, we have

$$\sigma_{i,j}^2 = \sum_{k=1}^{N_{meas}} w_k^2 \overline{LID}(i,j,k) \quad \text{(B18)}$$

which we can approximate by

$$\sigma_{i,j}^2 \approx \sum_{k=1}^{N_{meas}} w_k^2 LID(i,j,k) \quad \text{(B19)}$$

Appendix C. Geophysical model for the atmospheric return

C.1. Atmosphere return signal

To model the signal returned from the atmosphere by particles and molecules the standard lidar equation is adopted:

$$S^A(r) = \frac{C_A \beta^A(r)}{R^2} \exp\left[-2 \int_0^r \{\alpha^M(x) + \alpha^P(x)\} dx \right], \qquad \textbf{Eq. C1}$$

with *S* denoting the received signal as a function of *r*, the path along the laser beam (r=0 at the satellite), and *A* can be molecular (*M*) or particle (*P*). C_A denotes the calibration constant, β backscatter ($m^{-1}sr^{-1}$), *R* the range (m) from the atmosphere to the satellite along the laser beam and α the atmosphere extinction coefficient (m^{-1}).
For the vertical coordinate users generally prefer the altitude above mean sea level, denoted with *z*, of the location where the laser beam intersects the normal with the earth surface, rather than the sample range *r*, see Figure B. The rate of change of altitude with range is determined by the local incidence of the laser beam with respect to the Earth's normal, $\hat{\theta}$, as provided in the L1B product.

Eq. (C1) in the z-coordinate frame becomes

$$S^A(z) = \frac{C_A \beta^A(z)}{R^2(z)} \exp\left[-2 \int_z^h \frac{\{\alpha^M(x) + \alpha^P(x)\}}{\cos(\hat{\theta}(x))} dx \right], \qquad \textbf{Eq. C2}$$

where the range-to-height conversion is inserted in the integral and *h* is the satellite altitude. Define for the ADM range gate time sequence:

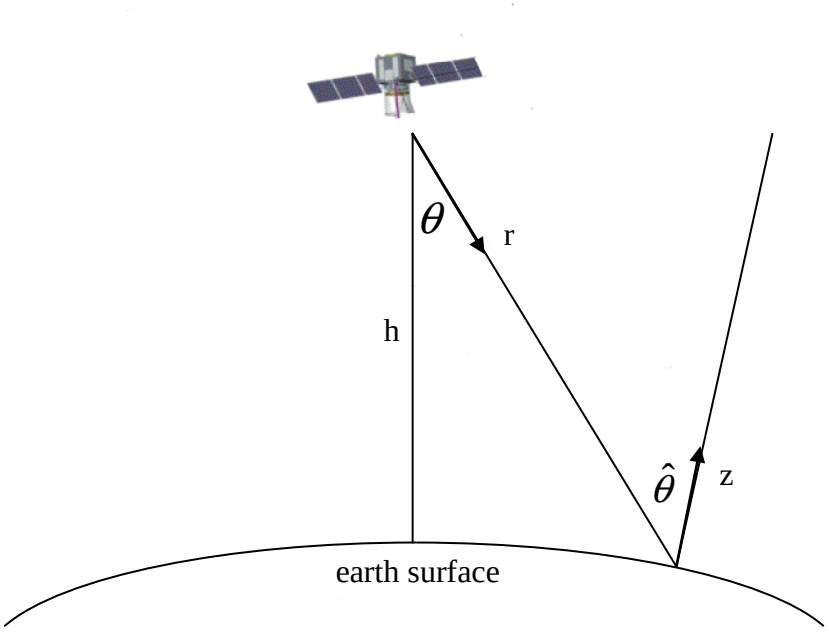

Figure B. ADM-Aeolus geometry.

$$S_i^A = \int_{z_i}^{z_{i-1}} S^A(y)dy$$

$$\int_{z_i}^{z_{i-1}} \frac{C_A \beta^A(y)}{R^2(y)} \exp\left[-2\int_{y}^{z+R(y)} \frac{\{\alpha^M(x)+\alpha^P(x)\}}{\cos(\hat{\theta}(x))}dx\right]dy \quad , \qquad i = 1,24$$

with the first bin (*i*=1) at the top of the DWL profile. Also define

- The range gate center: z_i^c
- $\hat{\theta}_i = \hat{\theta}(y)$, that is assumed constant over the range gate

We define integrated extinction α_i^A and backscatter β_i^A within the range gate with length $\Delta z_i = z_{i-1} - z_i$, according to

$$\alpha_i^A = \frac{1}{\Delta z_i}\int_{z_i}^{z_{i-1}} \alpha^A(x)dx\,, \qquad \beta_i^A = \frac{1}{\Delta z_i}\int_{z_i}^{z_{i-1}} \beta^A(x)dx\,.$$

We further obtain for one-way transmission through a range gate

$$\tau_i^A = \exp\left[\frac{-\alpha_i^A \Delta z_i}{\cos(\hat{\theta}_i)}\right] \qquad \textbf{Eq. C3}$$

For range gate *i* = 0 we assume transmissions τ_0^P and τ_0^M to account for respectively particle and molecular scatter between the satellite and the top of the DWL profile. We assume uniform extinction and backscatter conditions within the bin to solve the inner intergral of Eq. (2). Substituting in Eq. (C2) yields

$$S_i^A = \int_{z_i}^{z_{i-1}} \frac{C_A \beta^A(y)}{R^2(y)} \prod_{j=0}^{i-1}\left[\tau_j^P \tau_j^M\right]^2 \exp[\psi_i(z_{i-1}-y)]dy\,,$$

with $\psi_i = -2\left(\alpha_i^P + \alpha_i^M\right)/\cos\hat{\theta}_i$ defined for convenience. Solving the integral yields

$$S_i^A = \frac{C_A \beta_i^A}{R_i^2}\prod_{j=0}^{i-1}\left[\tau_j^P \tau_j^M\right]^2 \frac{-1}{\psi_i}[1-\exp\{\psi_i \Delta z_i\}] \qquad \textbf{Eq. C4}$$

Approximating the exponent through a truncated Taylor series expansion yields

$$S_i^A \approx \frac{C_A \beta_i^A}{R_i^2}\prod_{j=0}^{i-1}\left[\tau_j^P \tau_j^M\right]^2 \frac{-1}{\psi_i}\left[1-\left\{1+\psi_i \Delta z_i + \frac{1}{2}\psi_i{}^2 \Delta z_i{}^2\right\}\right]$$

$$= \frac{C_A \beta_i^A}{R_i^2}\prod_{j=0}^{i-1}\left[\tau_j^P \tau_j^M\right]^2 \Delta z_i\left\{1+\frac{\psi_i}{2}\Delta z_i\right\}$$

$$= \frac{C_A \beta_i^A}{R_i^2}\prod_{j=0}^{i-1}\left[\tau_j^P \tau_j^M\right]^2 \Delta z_i\left\{1-\frac{1}{\cos\hat{\theta}_i}\left(\alpha_i^P + \alpha_i^M\right)\Delta z_i\right\}$$

after backsubstitution of ψ_i. And after a similar but inverse Taylor expansion of the term in curly brackets we obtain

$$S_i^A \approx \frac{C_A \beta_i^A \Delta z_i}{R_i^2} \prod_{j=0}^{i-1} \left[\tau_j^P \tau_j^M\right]^2 \exp\left[\frac{-1}{\cos\hat{\theta}_i}\left(\alpha_i^P + \alpha_i^M\right)\Delta z_i\right]$$
$$= \frac{C_A \beta_i^A \Delta z_i}{R_i^2} \prod_{j=0}^{i-1} \left[\tau_j^P \tau_j^M\right]^2 \tau_i^P \tau_i^M \qquad \textbf{Eq. C5}$$

Eq. (C5) implies that the signal in layer *i* is on average half attenuated, i.e., signal originating from the top of the range bin is not attenuated within the layer, while at the bottom it is fully attenuated within the layer due to both down and up-ward propagation. This is consistent with the assumption that S_i represents the measured signal of the mid-point of the layer.

We note that sharp gradients in aerosol backscatter are aggregated through the ADM range gating principle and do affect the computation of the mean extinction and backscatter over a range gate. This effect is not addressed here. Instead the aggregated measurements at given range gate resolution are input to the optical computations and the Taylor expansion approximation. The impact of sharp backscatter gradients within a range bin interval, on the quality of the wind estimate (or the height assignment) in the case of substantial wind-shear over the integrated range gate, will be addressed specifically in the frame of ongoing sensitivity studies.

Approximation of the non-linear one-way signal transmission -[1-exp($\psi\Delta z$)]/$\psi\Delta z$ in Eq.(C4) with exp($\psi\Delta z$/2) (=$\tau^M\tau^P$) in Eq.(C5) through a forward and backward Taylor expansion of the exponential introduces an error that is a higher-order polynomial function of $\psi\Delta z$. An expression of the error is derived below. The full Taylor expansion of the non-linear one-way signal transmission yields

$$\frac{-1}{\psi\Delta z}(1-\exp(\psi\Delta z) = \frac{-1}{\psi\Delta z}\left[1-\left\{1+\psi\Delta z+\frac{\psi^2\Delta z^2}{2}+\sum_{n=3}^{\infty}\frac{(\psi\Delta z)^n}{n!}\right\}\right]$$
$$= 1+\frac{\psi\Delta z}{2}+\sum_{n=3}^{\infty}\frac{(\psi\Delta z)^{n-1}}{n!} \qquad \textbf{Eq. C6}$$

Also,

$$\tau_i^M \tau_i^P = \exp\left[\frac{-1}{\cos(\hat{\theta})}\left(\alpha_i^M + \alpha_i^P\right)\Delta z\right]$$
$$= \exp\left(\frac{\psi\Delta z}{2}\right) \qquad \textbf{Eq. C7}$$
$$= 1+\frac{\psi\Delta z}{2}+\sum_{n=2}^{\infty}\frac{\left(\frac{\psi\Delta z}{2}\right)^n}{n!}$$

The truncation error, ε_{trunc}, then follows directly from Eqs.(C6,C7):

$$\varepsilon_{\text{trunc}} = \frac{-1}{\psi\Delta z}(1-\exp(\psi\Delta z) - \tau_i^M\tau_i^P$$
$$= \sum_{n=3}^{\infty}\frac{(\psi\Delta z)^{n-1}}{n!} - \sum_{n=2}^{\infty}\frac{\left(\frac{\psi\Delta z}{2}\right)^n}{n!} \qquad \textbf{Eq. C8}$$
$$= \sum_{n=2}^{\infty}\frac{(\psi\Delta z)^n}{n!}\left[\frac{1}{n+1}-\left(\frac{1}{2}\right)^n\right]$$

The table below provides an indication of the amplitude of truncation error for a number of typical atmospheric scenes that are relevant for ADM.

	unit	Stratosphere (15km)	Free Troposphere (5 km)	Surface (0.5 km)	Cirrus (10 km)	Dust layer (2-6 km)
β^M	sr^{-1}	$1.0\ 10^{-6}$	$3.2\ 10^{-6}$	$6.3\ 10^{-6}$	$1.6\ 10^{-6}$	$4.0\ 10^{-6}$
α^M	m^{-1}	$8.4\ 10^{-6}$	$2.7\ 10^{-5}$	$5.3\ 10^{-5}$	$1.3\ 10^{-5}$	$3.4\ 10^{-5}$
β^P	sr^{-1}	$1.0\ 10^{-8}$	$3.2\ 10^{-8}$	$6.0\ 10^{-6}$	$2.1\ 10^{-5}$	$1.6\ 10^{-6}$
α^P	m^{-1}	$5.0\ 10^{-7}$	$1.6\ 10^{-6}$	$3.0\ 10^{-4}$	$2.1\ 10^{-4}$	$8.0\ 10^{-5}$
$-\psi$	m^{-1}	$2.22\ 10^{-5}$	$7.11\ 10^{-5}$	8.8410^{-4}	$5.58\ 10^{-4}$	$2.85\ 10^{-4}$
Δz	m	1000	1000	250	1000	1000
$-\psi\Delta z$	-	$2.22\ 10^{-2}$	$7.11\ 10^{-2}$	2.2110^{-1}	$5.58\ 10^{-1}$	$2.85\ 10^{-1}$
τ	-	0.989	0.965	0.90	0.77	0.87
ε_{trunc}	-	$2.03\ 10^{-5}$	$2.03\ 10^{-4}$	1.8210^{-3}	$9.85\ 10^{-3}$	$2.95\ 10^{-3}$
ε_{trunc}(%)	-	0.002	0.021	0.20	1.28	0.34

Table C2. Computation of the Taylor expansion truncation error for one-way signal transmission.

Several notes with respect to Table C1:

- Molecular and aerosol backscatter, β^M and β^P respectively, are obtained from Figure 2 of Marseille and Stoffelen (2003).
- Extinction, α, is computed from the backscatter through a backscatter-to-extinction ratio, κ: For molecular scattering κ^M equals $3/8\pi$ sr^{-1}. Typical values for particle backscatter are 0.02/0.04 sr^{-1} for urban/maritime aerosols and 0.1 sr^{-1} for cirrus clouds.
- The local incidence angle $\hat{\theta}$ is set to 37 degrees.
- Values for the one-way transmission, τ, correspond to the non-linear transmission expression, Eq. (C6).
- The characteristics from the dust layer are obtained from an Earlinet study near Lecce (It.) (de Tomassi et al., 2003).
- Propagation of truncation errors may potentially result in substantial errors in the lowermost bins. For a worst case scene of a cirrus layer at 10 km, a dust layer between 2 and 6 km and surface conditions in the range from 0-2 km and ignoring errors in the free troposphere, the true transmission equals $0.77*(0.87)^4*(0.9)^8=0.190$ and the approximated transmission $(0.77+9.85\ 10^{-3})*(0.87+2.95\ 10^{-3})^4*(0.9+1.82\ 10^{-3})^8=0.198$ or a 4.2% truncation error

In conclusion, the Taylor expansion approximation for one-way signal transmission is generally good enough for atmospheric scenes that are of interest for ADM. For the cirrus layer we may infer that for a layer with an optical thickness of 0.26 (-ln(0.77)) the error in the estimated optical thickness equals $-\ln(\tau)+\ln(\tau-\varepsilon_{trunc})=0.013$ or about 5%. This is probably small when compared to e.g. measurement noise and uncertainties in other optical parameters such as the particle backscatter-to-extinction ratio.
Only in cases of optically thick clouds (stratus, cumulus clouds), the approximation may fail giving large errors in the computation of the atmosphere optical properties. It has been argued that signal classification will be straightforward in these cases anyway and the lidar will generally not be able to penetrate such clouds, but this remains to be shown.

C.2. Atmosphere return signal measured by the instrument

Equation (C5) describes the total atmospheric return signal from molecules and particles. Only a fraction of these signals are measured by the double-FP and Fizeau units as outlined in e.g. [ILIAD, RD1]. The actually measured Rayleigh signal is obtained by summing the Rayleigh useful signals (that include both molecules and particles) in channels A and B of the double-FP Rayleigh receiver, see Eq.(1) in [RD1]. This equation may be rewritten by

$$S_{\mathrm{FP}}(i) = K_{\mathrm{ray}} C(\nu,P,T)\beta_i^M \frac{\Delta z_i}{R_i^2}\prod_{j=0}^{i-1}\left[\tau_j^P \tau_j^M\right]^2 \tau_i^P \tau_i^M$$
$$C(\nu,P,T) = C_1(\nu,P,T) + C_2(\nu)(\rho_i - 1) \qquad \textbf{Eq. C9}$$

with ρ_i the scattering ratio in bin *i*, that is defined as the fraction of total backscatter to molecular backscatter:

$$\rho_i = \frac{\beta_i^P + \beta_i^M}{\beta_i^M} = 1 + \frac{\beta_i^P}{\beta_i^M} \qquad \textbf{Eq. C10}$$

The calibration parameter $C_1(\nu,P,T)$ is determined from interpolating a Fabry-Perot (FP) lookup table. The lookup table has been generated using ILIAD output files. More specifically for a range of values for temperature, pressure and (Doppler shifted) frequency, the ILIAD software computes the Fabry-Perot signal from the molecular (Rayleigh-Brillioun) spectrum and FP channel transfer functions. At the moment no pressure dependence is available in the lookup table. Currently $C_2(\nu)$ is set to zero, pending further developments in the optical calibration, see [RD1].
For the scattering ratio several estimators exist that need further testing, as outlined below.

The actually measured Mie signal, on the Fizeau interferometer, is composed of a relative small peak, from atmosphere particle scattering, on top of a flat noise spectrum, from molecular scattering and background light. The Mie peak (S_i^P) is described with Eq.(C5), with C_P replaced by $K_{\mathrm{mie}}C_3(\nu)$, and the Rayleigh (background or noise) spectrum, N_{mie}, through (see [RD1])

$$S_{\mathrm{mie}}(i) = K_{\mathrm{mie}} C_3(\nu)\beta_i^P \frac{\Delta z_i}{R_i^2}\prod_{j=1}^{i-1}\left(\tau_j^M \tau_j^P\right)^2 \tau_i^M \tau_i^P$$
$$N_{\mathrm{mie}}(i) = K_{\mathrm{mie}} C_4(\nu,P,T)\beta_i^M \frac{\Delta z_i}{R_i^2}\prod_{j=1}^{i-1}\left(\tau_j^M \tau_j^P\right)^2 \tau_i^M \tau_i^P \qquad \textbf{Eq. C11}$$

The calibration parameters in C_3 and C_4 can in principle be determined from calibration measurements [RD1] and are assumed known in L2B. The total measured Mie signal is obtained by adding S_{mie} and N_{mie}.

Eqs.(C10),(C11) describe the measured signals by the instrument and are the basic equations for the retrieval of atmosphere optical properties in section 18.

C.3. The role of meteorological data in the geophysical model

Additional prior knowledge of the atmosphere is available from auxiliary NWP data and is used for the retrieval of atmosphere optical properties, in particular profiles of pressure, temperature and wind from NWP models. Molecular backscatter and extinction may be determined from Rayleigh theory given profiles of atmospheric pressure and temperature between the earth surface and satellite altitude as follows (Reagan et al. 1989).

$$\alpha^M(z) = \sigma_{\mathrm{mol}}(z) n(z)$$
$$\beta^M(z) = \frac{3}{8\pi}\alpha^M(z) \qquad \textbf{Eq. C12}$$
$$\tau^M(z) = \exp\left[\frac{-2}{\cos\hat{\theta}_i}\int_z^{z_L}\alpha^M(z)dz\right]$$

with α^M molecular extinction (m^{-1}), σ_{mol} the molecular scattering cross-section per molecule (m^2) and n the molecular number density that follows from the ideal gas law; $P(z)=n(z)kT(z)$, with P pressure in Pa, T temperature in degrees Kelvin and k the Boltzmann constant.

Appendix D. Checking of signal calibration factors

At the time of writing (May 2006) the calibration strategy for the Rayleigh and Mie channels is still an open issue. [RD1] provides a possible scheme showing that in principle, the calibration constants C_1, C_2, C_3, C_4, K_{ray} and K_{mie}, may be obtained from calibration measurements. C_1, is determined from a lookup table as outlined in section 3, K_{ray} is obtained from the two uppermost bins as outlined in section 5.1.

It was agreed at the L2B–PM5 meeting in March 2006 that the calibration constants are assumed as known input parameters in L2B, until more detailed information on the calibration procedure becomes available.

In this section a check on the calibration values is described using measured data in the Rayleigh and Mie channels.

D.1. Rayleigh channel signal calibration

Calibration of the Rayleigh channel is done on the measured Rayleigh signals in the first 2 bins, assuming no particles in these bins.

D.1.1. Input parameters

1 $S_{ray}(1)$ and $S_{ray}(2)$: the Rayleigh channel useful signal in the first and second bin from L1B;
2 τ_0^M : signal transmission through molecular scattering and absorption between the satellite and the first bin, from NWP data. This value will generally be very close to 1;
3 Molecular backscatter (β_1^M) and transmission (τ_1^M) within the first bin, from NWP data;
4 Calibration constant $C_1(v,T,P)$ from interpolating the lookup table, see section 3.
5 R_1 , R_2 , Δz_1 , Δz_2 , ε_{raycal}

D.1.2. Output parameters

1 K_{ray}: Rayleigh channel calibration value
2 A flag indicating the reliability of K_{ray}

D.1.3. Algorithm

An estimate of calibration factor K_{ray} may be obtained from the measured Rayleigh signal in the first bin, $S_{ray}(1)$, using Eq. (9) and assuming no particles between the satellite and second altitude bin, i.e. τ_0^P=1, τ_1^P=1 and β_1^P=0, ρ_1=1. Then from Eq. (9):

$$K_{ray} = \frac{S_{ray}(1) R_1^2}{\beta_1^M C_1 \Delta z_1 \left[\tau_0^M\right]^2 \tau_1^M} \qquad \textbf{Eq. D1}$$

since τ_0^M, τ_1^M and β_1^M are known for known temperature and pressure profiles, according to Eq. (C12).

The above algorithm provides a good calibration value only if the first bin is free of particles. This is verified by using the signal in the second bin. If both bins are free of particles then the ratio of both signals is independent of the calibration value and equals

$$\frac{S_{ray}(2)}{S_{ray}(1)} = \frac{\Delta z_2}{\Delta z_1} \frac{C_1(2)}{C_1(1)} \frac{R_1^2}{R_2^2} \frac{\beta_2^M}{\beta_1^M} \tau_1^M \tau_2^M$$

This "expected" ratio can be determined from NWP data. If the measured "true" ratio deviates more than a pre-defined threshold value, ε_{raycal}, from the expected value then this is an indication that either the first or second bin contains particles and a flag is set. (The reliability of the computed calibration factor may also be checked by comparing with calibration values from previous BRCs in a monitoring step, e.g. to detect the unlikely event that both bins are contaminated with particles.)

The percentage of cases that one of either bins is contaminated with particles will be checked for the atmospheric database in the sensitivity study.

Following further progress in the calibration strategy, more elaborated assumptions will be implemented.

D.2. Mie channel signal calibration

Calibration of the Mie channel is done using the measured molecular backscatter "noise floor" from the Fizeau interferometer. It is assumed that the first couple of bins in the stratosphere are (almost) free of particles, i.e. $S_{mie}(i) = 0$. This assumption will be verified with the expected signal ratio criterion from section 5.1. Then the total signal measured by the Mie channel is obtained from Eq.(11), with $\tau_i^P = 1$:

$$S_{\text{mie}}(i) = 0$$

$$N_{\text{mie}}(i) = K_{\text{mie}} C_4(\nu, P, T) \frac{\beta_i^M \Delta z_i}{R_i^2} \prod_{j=1}^{i-1} \left(\tau_j^M\right)^2 \tau_i^M$$

D.2.1. Input parameters

1 $S_{mie}(i) + N_{mie}(i)$: total Mie channel signal, from L1B
2 Molecular backscatter (β_i^M) and transmission (τ_i^M), from NWP data
3 C_4, from ?? (GJM, 22/05/2006)
4 R_i , Δz_i from L1B

D.2.2. Output parameters

1 K_{mie}: Mie channel calibration value

D.2.3. Algorithm

$$K_{\text{mie}}(i) = \frac{N_{\text{mie}}(i) R_i^2}{C_4 \beta_i^M \Delta z_i \prod_{j=1}^{i-1} \left(\tau_j^M\right)^2 \tau_i^M}$$

This computation can in principle be done for all altitude bins that are (almost) free of particles. This needs to be checked against the expected signal ratio criterion from section 5.1 and derived aerosol optical thickness in section 6. The vertical averaging of the resulting estimates to reduce measurement noise in the calibration estimate needs to be further investigated.

Appendix E. Computation of aerosol transmission from the Fabry-Perot channel signal

For a cloud-free atmospheric scene with aerosol attenuation but no aerosol backscatter an algorithm to compute particle transmission and subsequent particle extinction from the measured Fabry-Perot (FP) signal is described. We assume a background level of aerosols, e.g. the ADM-RMA aerosol backscatter profile of Vaughan, obtained from measurements in the relative clean atmosphere in 1989, before Pinatubo. Such an atmosphere is expected to generate negligible contamination of aerosol backscatter in the FP through cross-talk, in particular in the upper troposphere and stratosphere. In the described algorithm cross-talk is ignored.

First, a synthetic atmosphere containing molecules only is considered. Given temperature and pressure the expected signal on the FP receiver in bin *i*, $\hat{S}_{\mathrm{FP}}^{\mathrm{M}}(i)$ is determined from:

$$\hat{S}_{\mathrm{FP}}^{\mathrm{M}}(i) = K_{\mathrm{ray}} C_1(\nu, P, T)\beta^{\mathrm{M}}(i)\frac{\Delta z_i}{R_i^2}\prod_{j=0}^{i-1}\left[\tau^{\mathrm{M}}(j)\right]^2\tau^{\mathrm{M}}(i) \qquad \textbf{Eq. E-1}$$

The actually measured FP signal, $S_{\mathrm{FP}}(i)$, also includes signal loss through aerosol attenuation (scattering and absorption) and is modeled through Eq.(C9). In the stratosphere and for a background level of aerosol, the scattering ratio is close to 1 and thus $C \approx C_1$ in Eq. (C9).
Define $\mathrm{T}^{\mathrm{P}}(i)$ the one-way particle transmission between the satellite and the bottom of bin *i*:

$$\mathrm{T}^{\mathrm{p}}(i) = \prod_{j=0}^{i}\left[\tau^{\mathrm{p}}(j)\right] \qquad \textbf{Eq. E-2}$$

with, $\tau^{\mathrm{p}}(j)$ particle transmission in bin *j*. Then the measured FP channel signal is modeled from Eq.(9,E-1,E-2):

$$S_{\mathrm{FP}}(i) = \left(1-\varepsilon(i)\right)\hat{S}_{\mathrm{FP}}^{\mathrm{M}}(i)\overline{\mathrm{T}}^{\mathrm{p}^2}(i-1)\overline{\tau}^{\mathrm{p}}(i) \qquad \textbf{Eq. E-3}$$

with the overbar denoting the (unknown) true particle transmission and ε denoting model (e.g. Taylor approximation) and/or measurement error (e.g. noise). The following iterative (i.e. layer-stepping) scheme is proposed to retrieve particle transmission in bin *i* from the measured FP signal.

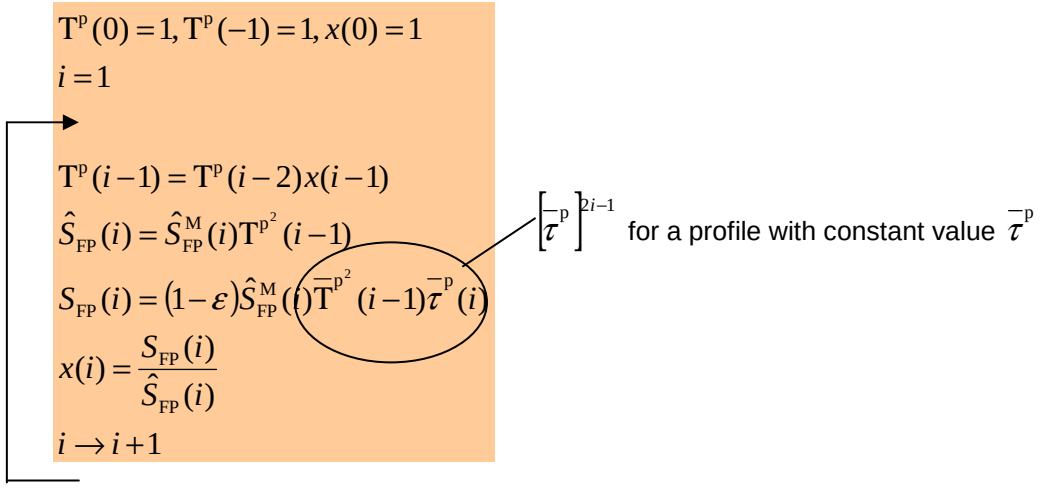

Figure E-1. Iterative scheme to retrieve particle transmission in bin *i*, from the measured Fabry-Perot signal, $S_{\mathrm{FP}}(i)$.

In the scheme in Fig. E-1, $\hat{S}_{\mathrm{FP}}(i)$ denotes the expected FP signal in bin *i* when there are no particles in bin *i*. The idea is that the quotient of the measured and expected FP signal in bin *i* (parameter *x*) provides an estimate of the particle transmission in bin *i*.
To study the behaviour of the scheme above, a simplified atmosphere is assumed with a constant aerosol transmission profile; $\bar{\tau}^{\mathrm{p}}(i)=\bar{\tau}^{\mathrm{p}}$ and thus $\bar{\mathrm{T}}^{\mathrm{p}}(i)=\left(\bar{\tau}^{p}\right)^{i}$. Also the error ε is assumed constant throughout the profile for simplicity. The solution of the scheme in Fig. E-1 with these assumptions is:

$$x(i)=\bar{\tau}^{\mathrm{p}}(1-\varepsilon)^{(-1)^{i+1}} \qquad i\geq 1 \qquad \textbf{Eq. E-4}$$

showing that the parameter *x* alternates around the true particle transmission value. Subsequent estimate for aerosol extinction follows from

$$\begin{aligned}\alpha^{\mathrm{p}}(i)&=\frac{-\ln(x(i))}{\Delta z}\\&=\frac{-\ln(\bar{\tau}^{\mathrm{p}})}{\Delta z}+\frac{(-1)^{i+1}\ln(1-\varepsilon)}{\Delta z}\\&\approx\frac{-\ln(\bar{\tau}^{\mathrm{p}})}{\Delta z}+\frac{(-1)^{i+1}\varepsilon}{\Delta z}\\&=\bar{\alpha}^{\mathrm{p}}(i)+\Delta\alpha^{\mathrm{p}}(i)\end{aligned} \qquad \textbf{Eq. E-5}$$

showing that the retrieved aerosol extinction obviously also alternates around the true value. This behaviour is visualized by the red curves in Fig. E-3.
From Eq. E-5, the relative error in the retrieved aerosol extinction equals $\left|\Delta\alpha^{\mathrm{p}}(i)\right|/\bar{\alpha}^{\mathrm{p}}(i)=|\varepsilon|/\ln(\bar{\tau}^{\mathrm{p}})$. Assuming no aerosol attenuation above 17.1 km, the iterative scheme implemented in L2B can be modeled with the scheme in Fig E-1 with ε=0.003. This error is mainly explained by a different resolution of the model atmosphere (125 meter) that is used to simulate S_{FP} (in E2S) and the DWL range gate resolution (typically 1000 meter). For a particle extinction value of 10^{-5} 1/m the one-way particle transmission equals $\bar{\tau}^{\mathrm{p}}=0.9875$ for a 1 km bin. Thus for this particular case a 0.3% error in the measured FP signal, gives a 23.8% error for the retrieved particle extinction, in agreement with the red curve in the left panel of Fig. E-3.

A solution to damp the alternating behaviour of the particle optical properties solution is obtained by the alternative scheme proposed in Fig. E-2 that only differs from Fig. E-1 through the power *k* that is applied to the computation of *x*.

$$\mathrm{T}^{\mathrm{p}}(0)=1,\mathrm{T}^{\mathrm{p}}(-1)=1,x(0)=1$$
$$i=1$$
$$\mathrm{T}^{\mathrm{p}}(i-1)=\mathrm{T}^{\mathrm{p}}(i-2)x(i-1)$$
$$\hat{S}_{\mathrm{FP}}(i)=\hat{S}^{\mathrm{M}}_{\mathrm{FP}}(i)\mathrm{T}^{\mathrm{p}^{2}}(i-1)$$
$$S_{\mathrm{FP}}(i)=(1-\varepsilon)\hat{S}^{\mathrm{M}}_{\mathrm{FP}}(i)\left[\bar{\tau}^{\mathrm{p}}\right]^{2i-1}$$
$$x(i)=\left[\frac{S_{\mathrm{FP}}(i)}{\hat{S}_{\mathrm{FP}}(i)}\right]^{k}$$
$$i\rightarrow i+1$$

Figure E-2. Same as Fig. E-1, but with a power *k* in the computation of parameter *x*.

The solution of the iterative scheme in Fig. E-2 is

$$x(j) = \bar{\tau}^{\beta(j,k)} \left\{ \left[(1-\varepsilon)\bar{\tau} \right]^{k} \right\}^{1-\beta(j,k)} \qquad \textbf{Eq. E-6}$$

with $\beta(j,k)$ a polynomial of k as follows

$$\beta(1,k) = 0$$
$$\beta(2,k) = 2k$$
$$\beta(3,k) = 4k - 4k^2$$
$$\beta(4,k) = 6k - 12k^2 + 8k^3$$
$$\beta(5,k) = 8k - 24k^2 + 32k^3 - 16k^4$$
$$\text{etc.}$$

A general expression for $\beta(j,k)$ is described later in the text. Here we constrain to the properties of $\beta(j,k)$

- for k=1, the value of $\beta(j,k)$ alternates between 0 and 2 and Eq. E-6 is in agreement with Eq. E-4.
- For k=1/2: $\beta(j,1/2)$=1 for j>0.
- $\lim_{j\to\infty} \beta(j,k) = 1, \quad \text{for } 0 < k < 1$

The last property implies that for suitable values of k, the impact of the error ε in the estimate for particle transmission damps with increasing j, i.e. further down into the profile. This is visualized in Fig. E-3 that shows aerosol extinction retrieval for different values of the power k.

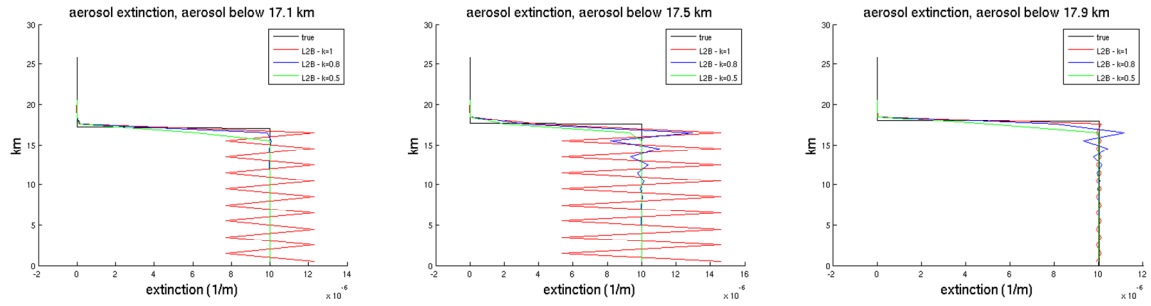

Figure E-3. L2B retrieval of aerosol extinction from the FP signal. No aerosol backscatter contamination is assumed. There is no aerosol attenuation at the top of the atmosphere. Aerosol extinction has a constant value of 10^{-5} 1/m (black lines) below 17.1 km (left panel) corresponding to a moderate value for ε, below 17.5 km (middle panel) corresponding to a large value for ε, and below 17.9 km (right panel) corresponding to a small value for ε. The red, blue and green lines show the L2B retrieval for k=1, 0.8 and 0.5 (see fig. E-2) respectively.

From Fig. E-3 it follows that the L2B aerosol optical properties retrieval depends on the position in the first range bin where substantial aerosol is found. This location determines the value of ε. In any case the solution for k=1 alternates around the true value, the amplitude depending on the location of aerosols within the first aerosol contaminated bin. For values of k smaller than one, the retrieved aerosol extinction converges to the true value at the expense of a bias in the first aerosol contaminated bin. This is explained later in the text.
Figure E-4 shows similar results for a linear increasing aerosol extinction.

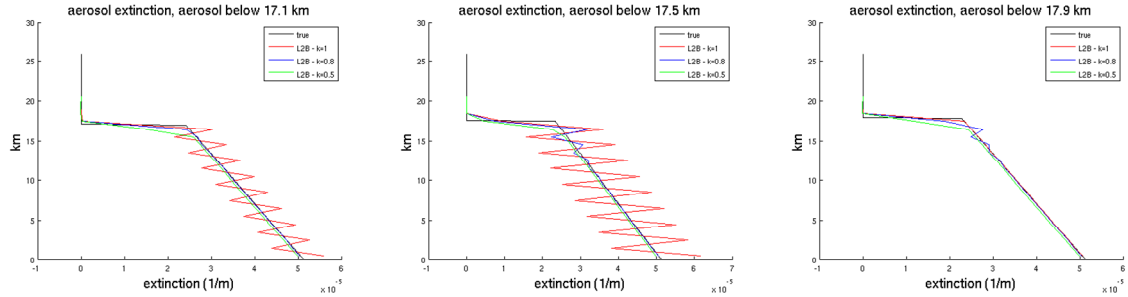

Figure E-4. Same as Fig. E-3, but now for a linear aerosol extinction.